Astronomy & Astrophysics manuscript no. aa29512-16
September 9, 2016

Gaia Data Release 1

Summary of the astrometric, photometric, and survey properties

Gaia Collaboration, A. G.A. Brown[1,⋆], A. Vallenari[2], T. Prusti[3], J. H.J. de Bruijne[3], F. Mignard[4], R. Drimmel[5], C. Babusiaux[6], C. A.L. Bailer-Jones[7], U. Bastian[8], M. Biermann[8], D. W. Evans[9], L. Eyer[10], F. Jansen[11], C. Jordi[12], D. Katz[6], S. A. Klioner[13], U. Lammers[14], L. Lindegren[15], X. Luri[12], W. O'Mullane[14], C. Panem[16], D. Pourbaix[17,18], S. Randich[19], P. Sartoretti[6], H. I. Siddiqui[20], C. Soubiran[21], V. Valette[16], F. van Leeuwen[9], N. A. Walton[9], C. Aerts[22,23], F. Arenou[6], M. Cropper[24], E. Høg[25], M. G. Lattanzi[5], E. K. Grebel[8], A. D. Holland[26], C. Huc[16], X. Passot[16], M. Perryman[3], L. Bramante[27], C. Cacciari[28], J. Castañeda[12], L. Chaoul[16], N. Cheek[29], F. De Angeli[9], C. Fabricius[12], R. Guerra[14], J. Hernández[14], A. Jean-Antoine-Piccolo[16], E. Masana[12], R. Messineo[27], N. Mowlavi[10], K. Nienartowicz[30], D. Ordóñez-Blanco[30], P. Panuzzo[6], J. Portell[12], P. J. Richards[31], M. Riello[9], G. M. Seabroke[24], P. Tanga[4], F. Thévenin[4], J. Torra[12], S. G. Els[32,8], G. Gracia-Abril[32,12], G. Comoretto[20], M. Garcia-Reinaldos[14], T. Lock[14], E. Mercier[32,8], M. Altmann[8,33], R. Andrae[7], T. L. Astraatmadja[7], I. Bellas-Velidis[34], K. Benson[24], J. Berthier[35], R. Blomme[36], G. Busso[9], B. Carry[4,35], A. Cellino[5], G. Clementini[28], S. Cowell[9], O. Creevey[4,37], J. Cuypers[36], M. Davidson[38], J. De Ridder[22], A. de Torres[39], L. Delchambre[40], A. Dell'Oro[19], C. Ducourant[21], Y. Frémat[36], M. García-Torres[41], E. Gosset[40,18], J.-L. Halbwachs[42], N. C. Hambly[38], D. L. Harrison[9,43], M. Hauser[8], D. Hestroffer[35], S. T. Hodgkin[9], H. E. Huckle[24], A. Hutton[44], G. Jasniewicz[45], S. Jordan[8], M. Kontizas[46], A. J. Korn[47], A. C. Lanzafame[48,49], M. Manteiga[50], A. Moitinho[51], K. Muinonen[52,53], J. Osinde[54], E. Pancino[19,55], T. Pauwels[36], J.-M. Petit[56], A. Recio-Blanco[4], A. C. Robin[56], L. M. Sarro[57], C. Siopis[17], M. Smith[24], K. W. Smith[7], A. Sozzetti[5], W. Thuillot[35], W. van Reeven[44], Y. Viala[6], U. Abbas[5], A. Abreu Aramburu[58], S. Accart[59], J. J. Aguado[57], P. M. Allan[31], W. Allasia[60], G. Altavilla[28], M. A. Álvarez[50], J. Alves[61], R. I. Anderson[62,10], A. H. Andrei[63,64,33], E. Anglada Varela[54,29], E. Antiche[12], T. Antoja[3], S. Antón[65,66], B. Arcay[50], N. Bach[44], S. G. Baker[24], L. Balaguer-Núñez[12], C. Barache[33], C. Barata[51], A. Barbier[59], F. Barblan[10], D. Barrado y Navascués[67], M. Barros[51], M. A. Barstow[68], U. Becciani[49], M. Bellazzini[28], A. Bello García[69], V. Belokurov[9], P. Bendjoya[4], A. Berihuete[70], L. Bianchi[60], O. Bienaymé[42], F. Billebaud[21], N. Blagorodnova[9], S. Blanco-Cuaresma[10,21], T. Boch[42], A. Bombrun[39], R. Borrachero[12], S. Bouquillon[33], G. Bourda[21], H. Bouy[67], A. Bragaglia[28], M. A. Breddels[71], N. Brouillet[21], T. Brüsemeister[8], B. Bucciarelli[5], P. Burgess[9], R. Burgon[26], A. Burlacu[16], D. Busonero[5], R. Buzzi[5], E. Caffau[6], J. Cambras[72], H. Campbell[9], R. Cancelliere[73], T. Cantat-Gaudin[2], T. Carlucci[33], J. M. Carrasco[12], M. Castellani[74], P. Charlot[21], J. Charnas[30], A. Chiavassa[4], M. Clotet[12], G. Cocozza[28], R. S. Collins[38], G. Costigan[1], F. Crifo[6], N. J.G. Cross[38], M. Crosta[5], C. Crowley[39], C. Dafonte[50], Y. Damerdji[40,75], A. Dapergolas[34], P. David[35], M. David[76], P. De Cat[36], F. de Felice[77], P. de Laverny[4], F. De Luise[78], R. De March[27], D. de Martino[79], R. de Souza[80], J. Debosscher[22], E. del Pozo[44], M. Delbo[4], A. Delgado[9], H. E. Delgado[57], P. Di Matteo[6], S. Diakite[56], E. Distefano[49], C. Dolding[24], S. Dos Anjos[80], P. Drazinos[46], J. Duran[54], Y. Dzigan[81,82], B. Edvardsson[47], H. Enke[83], N. W. Evans[9], G. Eynard Bontemps[59], C. Fabre[84], M. Fabrizio[55,78], S. Faigler[85], A. J. Falcão[86], M. Farràs Casas[12], L. Federici[28], G. Fedorets[52], J. Fernández-Hernández[29], P. Fernique[42], A. Fienga[87], F. Figueras[12], F. Filippi[27], K. Findeisen[6], A. Fonti[27], M. Fouesneau[7], E. Fraile[88], M. Fraser[9], J. Fuchs[89], M. Gai[5], S. Galleti[28], L. Galluccio[4], D. Garabato[50], F. García-Sedano[57], A. Garofalo[28], N. Garralda[12], P. Gavras[6,34,46], J. Gerssen[83], R. Geyer[13], G. Gilmore[9], S. Girona[90], G. Giuffrida[55], M. Gomes[51], A. González-Marcos[91], J. González-Núñez[29,92], J. J. González-Vidal[12], M. Granvik[52], A. Guerrier[59], P. Guillout[42], J. Guiraud[16], A. Gúrpide[12], R. Gutiérrez-Sánchez[20], L. P. Guy[30], R. Haigron[6], D. Hatzidimitriou[46], M. Haywood[6], U. Heiter[47], A. Helmi[71], D. Hobbs[15], W. Hofmann[8], B. Holl[10], G. Holland[9], J. A.S. Hunt[24], A. Hypki[1], V. Icardi[27], M. Irwin[9], G. Jevardat de Fombelle[30], P. Jofré[9,21], P. G. Jonker[93,23], A. Jorissen[17], F. Julbe[12], A. Karampelas[46,34], A. Kochoska[94], R. Kohley[14], K. Kolenberg[95,22,96], E. Kontizas[34], S. E. Koposov[9], G. Kordopatis[83,4], P. Koubsky[89], A. Krone-Martins[51], M. Kudryashova[35], I. Kull[85], R. K. Bachchan[15], F. Lacoste-Seris[59], A. F. Lanza[49], J.-B. Lavigne[59], C. Le Poncin-Lafitte[33], Y. Lebreton[6,97], T. Lebzelter[61], S. Leccia[79], N. Leclerc[6], I. Lecoeur-Taibi[30], V. Lemaitre[59], H. Lenhardt[8], F. Leroux[59], S. Liao[5,98], E. Licata[60], H. E.P. Lindstrøm[25,99], T. A. Lister[100], E. Livanou[46], A. Lobel[36], W. Löffler[8], M. López[67], D. Lorenz[61], I. MacDonald[38], T. Magalhães Fernandes[86], S. Managau[59], R. G. Mann[38], G. Mantelet[8], O. Marchal[6], J. M. Marchant[101], M. Marconi[79], S. Marinoni[74,55], P. M. Marrese[74,55], G. Marschalkó[102,103], D. J. Marshall[104], J. M. Martín-Fleitas[44], M. Martino[27], N. Mary[59], G. Matijevič[83], T. Mazeh[85], P. J. McMillan[15], S. Messina[49],

⋆ Corresponding author: A. G.A. Brown, e-mail: brown@strw.leidenuniv.nl

Article published by EDP Sciences, to be cited as http://dx.doi.org/10.1051/0004-6361/201629512

D. Michalik[15], N. R. Millar[9], B. M. H. Miranda[51], D. Molina[12], R. Molinaro[79], M. Molinaro[105], L. Molnár[102], M. Moniez[106], P. Montegriffo[28], R. Mor[12], A. Mora[44], R. Morbidelli[5], T. Morel[40], S. Morgenthaler[107], D. Morris[38], A. F. Mulone[27], T. Muraveva[28], I. Musella[79], J. Narbonne[59], G. Nelemans[23,22], L. Nicastro[108], L. Noval[59], C. Ordénovic[4], J. Ordieres-Meré[109], P. Osborne[9], C. Pagani[68], I. Pagano[49], F. Pailler[16], H. Palacin[59], L. Palaversa[10], P. Parsons[20], M. Pecoraro[60], R. Pedrosa[110], H. Pentikäinen[52], B. Pichon[4], A. M. Piersimoni[78], F.-X. Pineau[42], E. Plachy[102], G. Plum[6], E. Poujoulet[111], A. Prša[112], L. Pulone[74], S. Ragaini[28], S. Rago[5], N. Rambaux[35], M. Ramos-Lerate[113], P. Ranalli[15], G. Rauw[40], A. Read[68], S. Regibo[22], C. Reylé[56], R. A. Ribeiro[86], L. Rimoldini[30], V. Ripepi[79], A. Riva[5], G. Rixon[9], M. Roelens[10], M. Romero-Gómez[12], N. Rowell[38], F. Royer[6], L. Ruiz-Dern[6], G. Sadowski[17], T. Sagristà Sellés[8], J. Sahlmann[14], J. Salgado[54], E. Salguero[54], M. Sarasso[5], H. Savietto[114], M. Schultheis[4], E. Sciacca[49], M. Segol[115], J. C. Segovia[29], D. Segransan[10], I.-C. Shih[6], R. Smareglia[105], R. L. Smart[5], E. Solano[67,116], F. Solitro[27], R. Sordo[2], S. Soria Nieto[12], J. Souchay[33], A. Spagna[5], F. Spoto[4], U. Stampa[8], I. A. Steele[101], H. Steidelmüller[13], C. A. Stephenson[20], H. Stoev[117], F. F. Suess[9], M. Süveges[30], J. Surdej[40], L. Szabados[102], E. Szegedi-Elek[102], D. Tapiador[118,119], F. Taris[33], G. Tauran[59], M. B. Taylor[120], R. Teixeira[80], D. Terrett[31], B. Tingley[121], S. C. Trager[71], C. Turon[6], A. Ulla[122], E. Utrilla[44], G. Valentini[78], A. van Elteren[1], E. Van Hemelryck[36], M. van Leeuwen[9], M. Varadi[10,102], A. Vecchiato[5], J. Veljanoski[71], T. Via[72], D. Vicente[90], S. Vogt[123], H. Voss[12], V. Votruba[89], S. Voutsinas[38], G. Walmsley[16], M. Weiler[12], K. Weingrill[83], T. Wevers[23], Ł. Wyrzykowski[9,124], A. Yoldas[9], M. Žerjal[94], S. Zucker[81], C. Zurbach[45], T. Zwitter[94], A. Alecu[9], M. Allen[3], C. Allende Prieto[24,125,126], A. Amorim[51], G. Anglada-Escudé[12], V. Arsenijevic[51], S. Azaz[3], P. Balm[20], M. Beck[30], H.-H. Bernstein[†,8], L. Bigot[4], A. Bijaoui[4], C. Blasco[127], M. Bonfigli[78], G. Bono[74], S. Boudreault[24,128], A. Bressan[129], S. Brown[9], P.-M. Brunet[16], P. Bunclark[†,9], R. Buonanno[74], A. G. Butkevich[13], C. Carret[110], C. Carrion[57], L. Chemin[21,130], F. Chéreau[6], L. Corcione[5], E. Darmigny[16], K. S. de Boer[131], P. de Teodoro[29], P. T. de Zeeuw[1,132], C. Delle Luche[6,59], C. D. Domingues[133], P. Dubath[30], F. Fodor[16], B. Frézouls[16], A. Fries[12], D. Fustes[50], D. Fyfe[68], E. Gallardo[12], J. Gallegos[29], D. Gardiol[5], M. Gebran[12,134], A. Gomboc[94,135], A. Gómez[6], E. Grux[56], A. Gueguen[6,136], A. Heyrovsky[38], J. Hoar[14], G. Iannicola[74], Y. Isasi Parache[12], A.-M. Janotto[16], E. Joliet[39,137], A. Jonckheere[36], R. Keil[138,139], D.-W. Kim[7], P. Klagyivik[102], J. Klar[83], J. Knude[25], O. Kochukhov[47], I. Kolka[140], J. Kos[94,141], A. Kutka[89,142], V. Lainey[35], D. LeBouquin[59], C. Liu[7,143], D. Loreggia[5], V. V. Makarov[144], M. G. Marseille[59], C. Martayan[36,145], O. Martinez-Rubi[12], B. Massart[4,59,146], F. Meynadier[6,33], S. Mignot[6], U. Munari[2], A.-T. Nguyen[16], T. Nordlander[47], P. Ocvirk[83,42], K. S. O'Flaherty[147], A. Olias Sanz[148], P. Ortiz[68], J. Osorio[65], D. Oszkiewicz[52,149], A. Ouzounis[38], M. Palmer[12], P. Park[10], E. Pasquato[17], C. Peltzer[9], J. Peralta[12], F. Péturaud[6], T. Pieniluoma[52], E. Pigozzi[27], J. Poels[†,40], G. Prat[150], T. Prod'homme[1,151], F. Raison[152,136], J. M. Rebordao[133], D. Risquez[1], B. Rocca-Volmerange[153], S. Rosen[24,68], M. I. Ruiz-Fuertes[30], F. Russo[5], S. Sembay[68], I. Serraller Vizcaino[154], A. Short[3], A. Siebert[42,83], H. Silva[86], D. Sinachopoulos[34], E. Slezak[4], M. Soffel[13], D. Sosnowska[10], V. Straižys[155], M. ter Linden[39,156], D. Terrell[157], S. Theil[158], C. Tiede[7,159], L. Troisi[55,160], P. Tsalmantza[7], D. Tur[72], M. Vaccari[161,162], F. Vachier[35], P. Valles[12], W. Van Hamme[163], L. Veltz[83,37], J. Virtanen[52,53], J.-M. Wallut[16], R. Wichmann[164], M. I. Wilkinson[9,68], H. Ziaeepour[56], and S. Zschocke[13]

(Affiliations can be found after the references)

Received 10 August 2016 / Accepted 31 August 2016

ABSTRACT

Context. At about 1000 days after the launch of *Gaia* we present the first *Gaia* data release, *Gaia* DR1, consisting of astrometry and photometry for over 1 billion sources brighter than magnitude 20.7.

Aims. A summary of *Gaia* DR1 is presented along with illustrations of the scientific quality of the data, followed by a discussion of the limitations due to the preliminary nature of this release.

Methods. The raw data collected by *Gaia* during the first 14 months of the mission have been processed by the *Gaia* Data Processing and Analysis Consortium (DPAC) and turned into an astrometric and photometric catalogue.

Results. *Gaia* DR1 consists of three components: a primary astrometric data set which contains the positions, parallaxes, and mean proper motions for about 2 million of the brightest stars in common with the HIPPARCOS and *Tycho*-2 catalogues – a realisation of the *Tycho-Gaia* Astrometric Solution (TGAS) – and a secondary astrometric data set containing the positions for an additional 1.1 billion sources. The second component is the photometric data set, consisting of mean *G*-band magnitudes for all sources. The *G*-band light curves and the characteristics of ~3000 Cepheid and RR-Lyrae stars, observed at high cadence around the south ecliptic pole, form the third component. For the primary astrometric data set the typical uncertainty is about 0.3 mas for the positions and parallaxes, and about 1 mas yr^{-1} for the proper motions. A systematic component of ~0.3 mas should be added to the parallax uncertainties. For the subset of ~94 000 HIPPARCOS stars in the primary data set, the proper motions are much more precise at about 0.06 mas yr^{-1}. For the secondary astrometric data set, the typical uncertainty of the positions is ~10 mas. The median uncertainties on the mean *G*-band magnitudes range from the mmag level to ~0.03 mag over the magnitude range 5 to 20.7.

Conclusions. *Gaia* DR1 is an important milestone ahead of the next *Gaia* data release, which will feature five-parameter astrometry for all sources. Extensive validation shows that *Gaia* DR1 represents a major advance in the mapping of the heavens and the availability of basic stellar data that underpin observational astrophysics. Nevertheless, the very preliminary nature of this first *Gaia* data release does lead to a number of important limitations to the data quality which should be carefully considered before drawing conclusions from the data.

Key words catalogs – astrometry – parallaxes – proper motions – surveys

1. Introduction

The *Gaia* satellite was launched at the end of 2013 to collect data that will allow the determination of highly accurate positions, parallaxes, and proper motions for >1 billion sources brighter than magnitude 20.7 in the white-light photometric band G of *Gaia* (thus going deeper than the originally planned limit of $G = 20$). The astrometry is complemented by multi-colour photometry, measured for all sources observed by *Gaia*, and radial velocities which are collected for stars brighter than $G \approx 17$. The scientific goals of the mission are summarised in Gaia Collaboration et al. (2016b), while a more extensive scientific motivation for the mission is presented in Perryman et al. (2001).

The spacecraft, its scientific instruments, and the observing strategy have been designed to meet the performance requirement of 24 μas accuracy on the parallax of a 15th magnitude solar-type star at the end of the nominal 5 yr mission lifetime. The entity entrusted with the data processing for the *Gaia* mission, the *Gaia* Data Processing and Analysis Consortium (DPAC, described in Gaia Collaboration et al. 2016b), is expected to deliver the final data products (at their ultimately achievable accuracy) only at the end of post-operational phase of the mission, currently foreseen for 2022–2023. It was therefore agreed at the time of the creation of DPAC that the astronomical community should have access to the *Gaia* data at an earlier stage through intermediate data releases. It was understood that these intermediate releases are based on preliminary calibrations and only on a subset of the measurements available at the end of the mission, and therefore will not be representative of the end-of-mission *Gaia* performance.

In this paper we present the first such intermediate *Gaia* data release (*Gaia* Data Release 1, *Gaia* DR1), which is based on the data collected during the first 14 months of the nominal mission lifetime (60 months). In Sect. 2 we provide a short summary of the *Gaia* instruments and the way the data are collected. We summarise the astrometric, photometric and variable star contents of *Gaia* DR1 in Sect. 3. A summary of the validation of the results is provided in Sect. 4 and a few illustrations of the contents of *Gaia* DR1 are provided in Sect. 5. The known limitations of this first release are presented in Sect. 6. In Sect. 7 we provide pointers to the *Gaia* DR1 data access facilities and documentation available to the astronomical community. We conclude in Sect. 8. Although *Gaia* DR1 is the first major catalogue release with results from the *Gaia* mission, *Gaia* data has already been made publicly available as "Science Alerts" on transient sources, which for example led to the discovery of only the third known eclipsing AM CVn-system (Campbell et al. 2015).

We stress at the outset that *Gaia* DR1 represents a preliminary release of *Gaia* results with many shortcomings. We therefore strongly encourage a detailed reading of Sect. 6 and the documentation associated with the release as well as carefully taking into account the listed limitations when drawing conclusions based on the data contained in *Gaia* DR1.

2. *Gaia* instruments and measurements

We provide a brief overview of the *Gaia* instruments and the way measurements are collected in order to introduce some of the technical terms used in the rest of the paper. A full description of the *Gaia* spacecraft, instruments, and measurement principles can be found in Gaia Collaboration et al. (2016b).

Gaia continuously scans the sky with two telescopes pointing in directions separated by the basic angle of 106.5°. The images produced by the telescopes are projected onto the same focal plane composed of 106 CCDs which function as the detectors of the various instruments in the *Gaia* payload. The scanning is achieved through the continuous revolution of *Gaia* about its spin axis with a period of 6 h. The spin axis direction precesses around the direction to the Sun (as seen from *Gaia*), which allows complete coverage of the sky. Statistics of the sky coverage achieved for *Gaia* DR1 are presented in Lindegren et al. (2016) and van Leeuwen et al. (2016), while the properties of the *Gaia* scanning law with respect to variable star studies are described in Eyer et al. (2016).

The spinning motion of the spacecraft results in the source images moving across the focal plane. This necessitates the operation of the *Gaia* CCDs in time-delayed integration (TDI) mode so as to allow the accumulation of charge as the images move across the CCDs. The CCDs are not fully read out, only the pixels in a "window" around each source are read out and stored for transmission to the ground. These windows come in various sizes and sampling schemes.

The astrometric instrument takes up most of the focal plane and collects source images in the *Gaia* white-light pass band G (covering the range 330–1050 nm, Carrasco et al. 2016; Jordi et al. 2010). The fundamental inputs to the astrometric data processing consist of the precise times when the image centroids pass a fiducial line on the CCD (Lindegren et al. 2012). The image centroid and the flux contained in the image are determined as part of the pre-processing (Fabricius et al. 2016). The sensitivity of the astrometric instrument is such that sources brighter than about $G = 12$ will lead to saturated images. This effect is mitigated through the use of TDI gates, which are special structures on the CCDs that can be activated to inhibit charge transfer and hence to effectively reduce the integration time for bright sources.

The photometric instrument is realised through two prisms dispersing the light entering the field of view of two dedicated sets of CCDs. The Blue Photometer (BP) operates over the wavelength range 330–680 nm, while the Red Photometer (RP) covers the wavelength range 640–1050 nm (Carrasco et al. 2016; Jordi et al. 2010). The data collected by the photometric instrument consists of low resolution spectrophotometric measurements of the source spectral energy distributions. This colour information is intended for use in the astrometric processing (to correct for chromatic effects) and to provide the astrophysical characterisation of all sources observed by *Gaia*. The G-band photometry is derived from the fluxes measured in the astrometric instrument. Results from the photometric instrument are not presented as part of *Gaia* DR1. The photometry in this first release only concerns the fluxes measured in the G band.

The spectroscopic instrument, also called the radial-velocity spectrometer (RVS) collects medium resolution ($R \sim 11\,700$) spectra over the wavelength range 845–872 nm, centred on the Calcium triplet region (Cropper & Katz 2011). The spectra are collected for all sources to $G \approx 17$ (16th magnitude in the RVS filter band) and serve primarily to determine the radial velocity of the sources, although at the bright end ($G < 12.5$, Recio-Blanco et al. 2016) astrophysical information can be derived directly from the spectra. Results from this instrument are not contained in *Gaia* DR1.

Observations of sources by *Gaia* can be referred to in several ways. "Focal plane transits" refer to a crossing of the entire focal plane by a given source, which corresponds to a "visit" by *Gaia* of a specific coordinate on the sky. "CCD transits" refer to the crossing by a source of a particular CCD in the focal plane. Thus the focal plane transit of the astrometric field typically consists

of 10 transits across individual CCDs, while a photometric instrument transit (BP or RP) consists of only one CCD transit, and a transit across the RVS instrument consists of three CCD transits (see Gaia Collaboration et al. 2016b; Crowley et al. 2016b, for more details on the focal plane layout and functionalities, and the in-flight performance of the *Gaia* CCDs). This distinction is important when it comes to the difference between the number of measurements (CCD transits) collected for a source and the number of times it was observed (focal plane transits) by *Gaia*. In the rest of the paper we will refer to an "observation" or a "focal plane transit" to indicate that a source was observed by *Gaia* and we refer to "CCD transit" whenever individual CCD measurements are discussed.

Events on board *Gaia* are labelled by the so-called on board mission time line (OBMT), which is a time scale defined by the on board clock. This time scale is eventually transformed into the physical barycentric coordinate time (TCB) (Gaia Collaboration et al. 2016b; Lindegren et al. 2016). By convention OBMT is expressed in units of 6 h (21 600 s) spacecraft revolutions since launch and this unit is often used in figures of some quantity versus time, including in the papers accompanying *Gaia* DR1 and in the data release documentation (see Sect. 7). For the practical interpretation of time lines expressed in OBMT the following approximate relation between the OBMT (in revolutions) and TCB at *Gaia* (in Julian years) can be used:

$$\mathrm{TCB} \simeq \mathrm{J2015.0} + (\mathrm{OBMT} - 1717.6256\ \mathrm{rev})/(1461\ \mathrm{rev}). \quad (1)$$

This relation is precise to ±2 s and is valid only for the time span corresponding to *Gaia* DR1. The time interval covered by the observations used for *Gaia* DR1 starts at OBMT 1078.3795 rev = J2014.5624599 TCB (approximately 2014 July 25, 10:30:00 UTC), and ends at OBMT 2751.3518 rev = J2015.7075471 TCB (approximately 2015 September 16, 16:20:00 UTC), thus spanning 418 days. This time interval contains a significant number of gaps which are caused by: events or operations on board *Gaia* that prevent the collection of data or make the raw data unusable for a while (such as the decontamination of the payload); problems in the pre-processing leading to effective gaps in the available raw *Gaia* data (which has to be reconstructed from the raw telemetry, Fabricius et al. 2016); gaps in the spacecraft attitude solution deliberately introduced around the times when micro-meteoroid hits occurred (Lindegren et al. 2016). Telemetry losses along the spacecraft to ground link are only a very minor contribution to the data gaps. As a result of these gaps the amount of data processed for *Gaia* DR1 comprises slightly less than 12 (out of the above mentioned 14) months. The data gaps inevitably affect the quality of the *Gaia* DR1 results. In future releases the gaps related to the on-ground processing will disappear.

3. Overview of the contents of *Gaia* DR1

Gaia DR1 contains astrometry, *G*-band photometry, and a modest number of variable star light curves, for a total of 1 142 679 769 sources. Basic statistics for *Gaia* DR1 are listed in Table 1. The three main components of *Gaia* DR1 are:

1. The *astrometric data set* which consists of two subsets:
   The *primary astrometric data set* contains the positions, parallaxes, and mean proper motions for 2 057 050 stars in common between the *Gaia* DR1, HIPPARCOS and *Tycho*-2 catalogues. This data set represents the realisation of the *Tycho-Gaia* astrometric solution (TGAS), of which the principles were outlined and demonstrated in Michalik et al. (2015). The typical uncertainty is about 0.3 mas for the positions, and about 1 mas yr^{-1} for the proper motions. For the subset of 93 635 HIPPARCOS stars in the primary astrometric data set the proper motions are much more precise, at about 0.06 mas yr^{-1}. The typical uncertainty for the parallaxes is 0.3 mas, where it should be noted that a systematic component of ∼0.3 mas should be added (see Sect. 6).
   The *secondary astrometric data set* contains the positions for an additional 1 140 622 719 sources. For the secondary data set the typical uncertainty on the positions is ∼10 mas.
   The positions and proper motions are given in a reference frame that is aligned with the International Celestial Reference Frame (ICRF) to better than 0.1 mas at epoch J2015.0, and non-rotating with respect to ICRF to within 0.03 mas yr^{-1}. The detailed description of the production of the astrometric solution, as well as a more detailed statistical summary of the astrometry contained in *Gaia* DR1 can be found in Lindegren et al. (2016). An in-depth discussion of the *Gaia* DR1 reference frame and the optical properties of ICRF sources is presented in Mignard et al. (2016).
2. The *photometric data set* contains the mean *Gaia* *G*-band magnitudes for all the sources contained in *Gaia* DR1. The brightest source in *Gaia* DR1 has a magnitude $G = 3.2$, while the majority of the sources (99.7%) are in the range $11.2 \leq G \leq 21$. The small fraction of sources at $G > 21$ (where the nominal survey limit is $G = 20.7$, Gaia Collaboration et al. 2016b) most likely have erroneously determined *G*-band fluxes, but nevertheless passed the data quality filters described in Sect. 4. The typical uncertainties quoted on the mean value of *G* range from a millimagnitude or better at the bright end ($G \lesssim 13$), to about 0.03 mag at the survey limit. The details of the photometric data set, including the data processing and validation of the results is described in van Leeuwen et al. (2016), Carrasco et al. (2016), Riello et al. (2016), Evans et al. (2016).
3. The *Cepheids and RR Lyrae data set* contains the *G*-band light curves and characteristics of a modest sample of 599 Cepheid (43 newly discovered) and 2595 RR-Lyrae (343 new) variables located around the south ecliptic pole and observed at high cadence during a special scanning

Table 1. Basic statistics on the contents of *Gaia* DR1.

Source numbers	
Total number of sources	1 142 679 769
No. of primary (TGAS) sources	2 057 050
HIPPARCOS	93 635
Tycho-2 (excluding HIPPARCOS stars)	1 963 415
No. of secondary sources	1 140 622 719
No. of sources with light curves	3194
Cepheids	599
RR Lyrae	2595
Magnitude distribution percentiles (*G*)	
0.135%	11.2
2.275%	14.5
15.866%	17.1
50%	19.0
84.134%	20.1
97.725%	20.7
99.865%	21.0

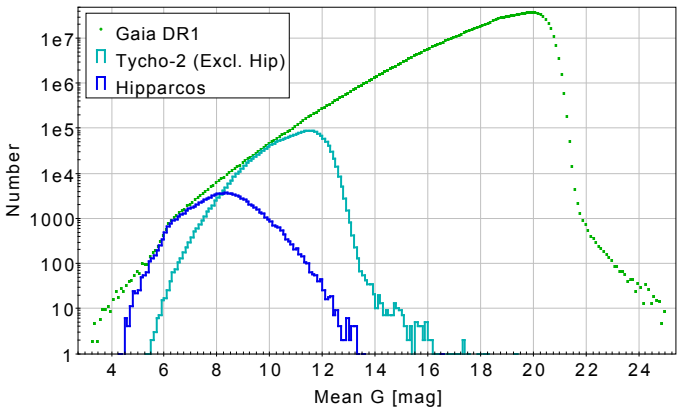

Fig. 1. Distribution of the mean values of G for all *Gaia* DR1 sources shown as histograms with 0.1 mag wide bins. The distributions for the HIPPARCOS and *Tycho*-2 (excluding the HIPPARCOS stars) subsets are also shown. Note the lack of bright sources at $G \lesssim 7$.

period in the first four weeks of the operational phase of *Gaia*. The variable star contents of *Gaia* DR1 are described in detail in Eyer et al. (2016) and Clementini et al. (2016).

The distribution of the sources in magnitude is shown in Fig. 1. The magnitude distribution of the sources reveals a drop-off at $G \lesssim 7$. Neither all HIPPARCOS nor all *Tycho*-2 sources are included in *Gaia* DR1 and at the faint end the magnitude limit is sky position dependent and ill-defined. At magnitudes below $G \sim 5$ the total number of sources in *Gaia* DR1 is larger than the number of HIPPARCOS sources in *Gaia* DR1. This is however only apparent as most of these sources are in fact in common with the HIPPARCOS catalogue but have been treated as secondary astrometric sources, because a good 5-parameter astrometric solution could not be derived. The limitations of *Gaia* DR1, including its completeness, are discussed in Sect. 6.

Of the 1141 million sources in the secondary astrometric data set 685 million are in common with the Initial *Gaia* Source List (IGSL, Smart & Nicastro 2014) and 456 million are new sources (Lindegren et al. 2016). The IGSL formed the starting point for the process of assigning *Gaia* observations to sources (Fabricius et al. 2016). Hence the term "new" should strictly speaking be interpreted as referring to sources that could not be matched to known IGSL sources. No attempt was made to establish how many sources are truly new discoveries by *Gaia* but this is likely to be a substantial fraction (over 400 million) of the new sources mentioned above. The IGSL has been publicly available for some time and we caution that when looking up a source in *Gaia* DR1 through its already known IGSL source identifier, it should be kept in mind that a large fraction of the 1.2 billion sources in the IGSL does not appear in *Gaia* DR1.

4. *Gaia* DR1 validation and source filtering

A substantial effort was dedicated to the validation of the results contained in *Gaia* DR1. This is a complex task which takes place at various levels within the DPAC. The outputs produced by the DPAC subsystems (described in Gaia Collaboration et al. 2016b) are validated first through an "internal" quality control process. For the astrometric data set in *Gaia* DR1 this internal validation is described in Lindegren et al. (2016), while that for the photometric and variable star data sets is described in (Evans et al. 2016) and Eyer et al. (2016), respectively. A second validation stage is carried out by the DPAC unit responsible for the data publication (cf. Gaia Collaboration et al. 2016b), which examines all the data contained in *Gaia* DR1 together and thus provides an independent quality check. This global validation process is described in Arenou et al. (2016). Here we summarise only the most important findings from the validation and provide complementary illustrations of the quality of *Gaia* DR1 in Sect. 5.

Numerous tests were done during the validation stage of the *Gaia* DR1 production, ranging from basic consistency checks on the data values to the verification that the data is scientifically correct. No problems were revealed that would prevent the timely publication of *Gaia* DR1. However, a number of minor problems were found that have been addressed either by a filtering of the available DPAC outputs before their incorporation into the data release, or by documenting the issues found as known limitations to *Gaia* DR1 (see Sect. 6). The filtering applied to the astrometric and photometric processing outputs before the global validation stage was as follows:

- For the primary astrometric data set only sources for which the standard uncertainties on the parallaxes and positions are less than 1 mas and 20 mas, respectively, were kept. In addition it was required that the sources have valid photometric data. For the secondary astrometric data set the sources were filtered by requiring that they were observed by *Gaia* at least 5 times (i.e. at least 5 focal plane transits), and that their astrometric excess noise (which indicates the astrometric modelling errors for a specific source) and position standard uncertainty are less than 20 mas and 100 mas, respectively. More details can be found in Lindegren et al. (2016). We stress that no filtering was done on the actual value of the source astrometric parameters.
- Although the photometric results were not explicitly filtered before their incorporation into *Gaia* DR1, a number of filters internal to the photometric data processing effectively leads to filtering at the source level. In particular sources with extremely blue or red colours will not appear in *Gaia* DR1.
- The only filtering done on the outputs of the variable star processing was to remove a handful of sources that were very likely a duplicate of some other source (see below for more discussion on duplicate sources).

The second validation stage (Arenou et al. 2016) revealed the following problems that were addressed through a further filtering of the astrometric and photometric processing outputs before their final incorporation into *Gaia* DR1. The filters described below were thus applied after the filters above.

- Some 37 million source pairs were found which are separated by less than 1 *Gaia* focal plane pixel size on the sky (i.e. 59 mas), or are separated by less than 5 times their combined positional standard uncertainty (where the factor 5 accounts for a possible underestimation of the standard uncertainties). The vast majority of these pairs are created during the cross-match stage, when observations (focal plane transits) get grouped together and assigned to sources (see Fabricius et al. 2016). The main underlying cause is sources appearing twice in the IGSL, which was evident from the many close pairs occurring along photographic survey plate boundaries (the IGSL is based to a large extent on photographic surveys, Smart & Nicastro 2014). A large fraction of these pairs are likely to be two instances of the same physical source (i.e. the source appears twice in the *Gaia* source list with two different identifiers). One member of each of these close pairs was filtered out of the *Gaia* DR1 source list

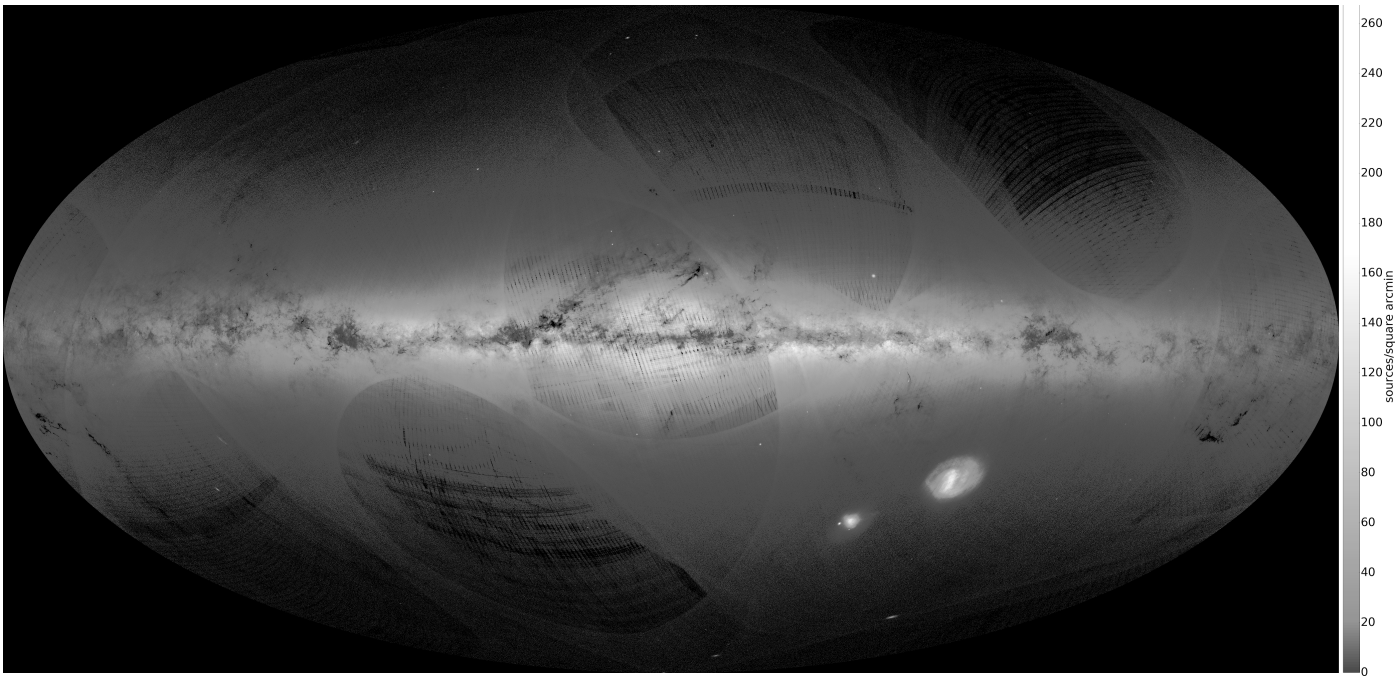

Fig. 2. Sky distribution of all *Gaia* DR1 sources in Galactic coordinates. The source density is shown with a grey scale chosen to highlight both the impressive amount of detail in the outlines of the well known dust features along the Galactic plane, and the non-astronomical artefacts in the source distribution (see text). Image credits: CENTRA − University of Lisbon (part of the DPAC-CU9 visualisation team).

and the remaining sources were flagged as having a duplicate associated to them in the *Gaia* source list. This flag thus indicates that the source in question has fewer observations contributing to its astrometry and photometry because part of the observations were assigned to another (fictitious) source. This filtering will in a fraction of the cases inevitably have removed one component from a real double source (be it a binary or an optical pair). This problem of duplicate sources will disappear in future *Gaia* data releases due to improvements in the cross-match algorithm and the moving away from the Initial *Gaia* Source List as the basis for assigning observations to sources.

– For some 1 million sources the mean G values were grossly inconsistent with either existing photometry (for example some TGAS stars were assigned G-band magnitudes much fainter than the *Tycho*-2 survey limit) or with the broad-band $G_{\rm BP}$ and $G_{\rm RP}$ magnitudes determined from the *Gaia* Blue and Red Photometers. In either case data processing problems are indicated and sources were removed from *Gaia* DR1 when there were fewer than 11 measurements in the G band (i.e. CCD transits in the astrometric part of the focal plane), or if both $(G - G_{\rm BP})$ and $(G - G_{\rm RP})$ were larger than +3.

Although the filtering described above will have removed the vast majority of problem cases from the DPAC outputs before the publication of *Gaia* DR1, it will nevertheless not be perfect. Genuine sources will have been removed and the filtering criteria do not guarantee the absence of a small fraction of problematic sources in *Gaia* DR1.

The decision to filter out the problematic cases rather than publish them with, e.g. indicator flags, was driven by data quality considerations and by the need to remove the large number of spurious sources created in the process of matching observations to sources (see Fabricius et al. 2016; Lindegren et al. 2016). The filtering thus reflects the preliminary nature of the first *Gaia* data release. In future intermediate releases the shortcomings in the data processing will be addressed and more measurements will be added, which means that reliable results can be derived for more sources. The level of filtering is thus expected to go down and more sources will enter the published catalogue.

5. Illustrations of the *Gaia* DR1 contents

Here we provide a few illustrations of the contents of *Gaia* DR1. The purpose is not to provide a scientific analysis but to demonstrate through astronomically relevant examples the overall quality of the *Gaia* data. A more detailed examination of the scientific quality of *Gaia* DR1 is provided in two studies on open clusters (*Gaia* Collaboration et al. 2016c) and the Cepheid period-luminosity relation (Gaia Collaboration et al. 2016a). We end this section with a comment on the Pleiades cluster distance.

5.1. The Gaia sky

The distribution of all *Gaia* DR1 sources on the sky is illustrated in Fig. 2. The source density shown in Fig. 2 is based on the accurate positions of the 1.1 billion sources in *Gaia* DR1 and represents the most detailed all-sky map in the optical to date. This can be appreciated in particular in the very fine outlining of the dust features along the Galactic plane. Also noteworthy are the Magellanic clouds, where in the Large Magellanic Cloud the individual features in the star forming regions north of the bar are outlined in the source distribution; the M31 and M33 galaxies which are both outlined in individual detections made by *Gaia*; and the Orion A and B clouds which can be seen against the backdrop of the sources detected by *Gaia*. Also recognisable are globular clusters, such as ω Centauri with over two hundred thousand sources individually appearing in *Gaia* DR1, and the Fornax dwarf spheroidal galaxy (∼30 000 sources in *Gaia* DR1) near $(\ell, b) \approx (237°, -66°)$. The full detail of this sky map is impossible to convey in print. An interactive and zoomable version will be available, through the Aladin sky atlas application

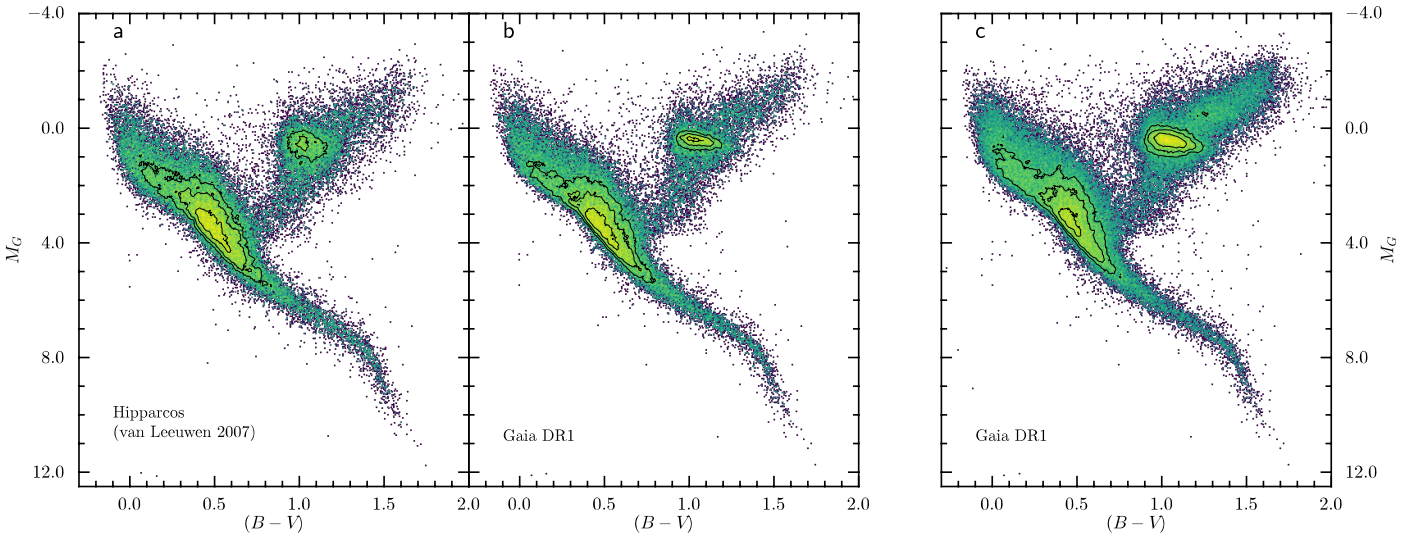

Fig. 3. Comparison of the observational HR diagram in the M_G vs. $(B-V)$ plane for the HIPPARCOS stars in *Gaia* DR1, using their HIPPARCOS (van Leeuwen 2007) parallaxes **a)** and their parallaxes as listed in *Gaia* DR1 **b)**, **c)**. The relative standard uncertainties on the parallax are less than 20% for both the HIPPARCOS and *Gaia* DR1 parallaxes in panels **a)** and **b)**, while in panel **c)** all stars with relative parallax uncertainties better than 20% in *Gaia* DR1 are shown. The stars were otherwise selected as described in the text. All panels show the stars as individual symbols where possible and where the symbols overlap the relative source density is shown, with colours varying from purple (dark) to yellow (light) indicating increasing density on a logarithmic scale. The contours enclose 10, 30, and 50 per cent of the data.

(Bonnarel et al. 2000; Boch & Fernique 2014) and a dedicated visualisation service, both as part of the *Gaia* data access facilities (see Sect. 7). The sky map also reveals a number of prominent non-astronomical artefacts which reflect the preliminary nature of the first *Gaia* data release. They are further discussed in Sect. 6.

The depth of the *Gaia* survey, its all-sky reach, the high angular resolution, combined with the highly accurate source positions, promises a revival of classical star count studies, in particular with future *Gaia* data releases where the shortcomings in the completeness and angular resolution of *Gaia* DR1 (see Sect. 6) will have been addressed. The *Gaia* sky map is also of immediate interest to studies of minor solar system bodies through stellar occultations, the predictions of occultation tracks on the earth benefiting from the dense distribution of sources with accurately known positions.

Finally, the *Gaia* sky map will be the standard reference in the optical for some time to come, in particular when in future releases the *Gaia* catalogue will be more complete in sky, magnitude, and colour coverage, and the source positions are further refined, with parallaxes and proper motions becoming available for all *Gaia* sources. This is to the benefit of all (optical) telescope guidance applications, especially large-mirror telescopes with small fields of view. Space missions will also benefit from the *Gaia* sky map. As an example, it is planned to improve the recently released Hubble Source Catalog (Whitmore et al. 2016) through a re-reduction of the astrometry with respect to the *Gaia* source positions.

5.2. Hertzsprung-Russell diagrams based on Gaia DR1 parallaxes

With the advent of *Gaia* DR1 we now for the first time have access to two large samples of parallaxes accurate at the (sub-) milliarcsecond level. As explained in Lindegren et al. (2016) the *Gaia* and HIPPARCOS parallaxes are independent and can thus sensibly be compared to each other. The comparison described in the appendix of Lindegren et al. (2016) shows that overall the *Gaia* DR1 and HIPPARCOS parallaxes are the same to within the combined uncertainties. A closer look at the parallaxes near zero reveals that for the HIPPARCOS stars in *Gaia* DR1 the number of negative parallaxes is much smaller, which is expected for a data set that is more precise. This comparison is furthermore exploited in Lindegren et al. (2016) to derive the relation between the formal and actual (published) uncertainties for the astrometric source parameters in the primary astrometric data set of *Gaia* DR1.

We illustrate the better overall precision of the *Gaia* parallaxes by constructing observational Hertzsprung-Russell (HR) diagrams in M_G vs. $(B-V)$ using the HIPPARCOS parallaxes from van Leeuwen (2007) and the parallaxes from *Gaia* DR1. The result is shown in Fig. 3. The 43 546 HIPPARCOS stars included in the left two panels a and b were selected according to:

$$(\varpi/\sigma_\varpi)_{Gaia} \geq 5 \quad \wedge \quad (\varpi/\sigma_\varpi)_{\text{HIPPARCOS}} \geq 5 \quad \wedge \quad \sigma_G \leq 0.05 \quad \wedge \quad \sigma_{(B-V)} \leq 0.05, \tag{2}$$

where ϖ is the parallax and σ_ϖ the corresponding standard uncertainty. The values of $(B-V)$ and their standard uncertainties were taken from the HIPPARCOS Catalogue (van Leeuwen 2007). The 74 771 stars in the rightmost panel (c) were selected only on the value of the relative uncertainty in the *Gaia* DR1 parallax but with the same criteria on the uncertainty in G and $(B-V)$. The median *Gaia* DR1 parallax for the smaller sample is 7.5 and for the larger sample it is 5.0 mas, while 90 per cent of the stars have a parallax larger than 3.6 (smaller sample) and 2.2 mas (larger sample). A comparison of the left two panels shows that with the *Gaia* DR1 parallaxes the main sequence is better defined, being somewhat narrower and with a sharper boundary along the faint end. The distribution of red clump giants is much narrower in luminosity, with the effect of extinction and reddening clearly seen as an elongation in the direction of fainter magnitudes and redder colours.

The narrower luminosity distribution of the red clump giants and main sequence dwarfs in *Gaia* DR1 is further illustrated in Fig. 4. The luminosity distribution is shown for the stars

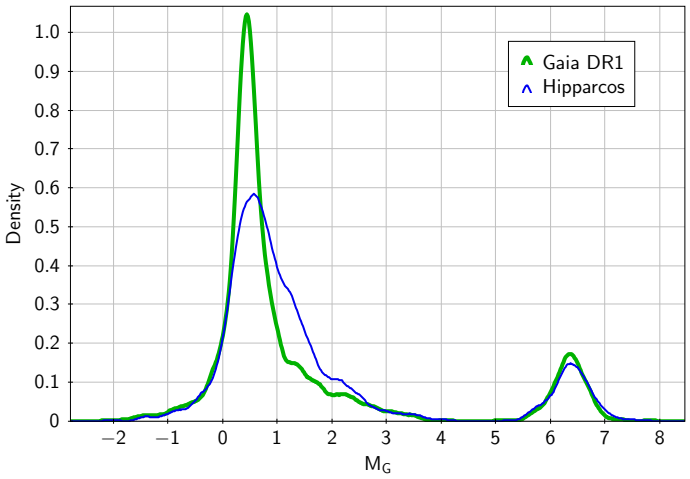

Fig. 4. Distribution of absolute magnitudes M_G for the stars from Fig. 3 (panels **a)** and **b)**) within the colour range $1.0 \leq (B-V) \leq 1.1$. The thick green solid line shows the distribution of M_G derived from *Gaia* DR1 parallaxes, while the thin blue line shows the same for the HIPPARCOS parallaxes. The distributions are represented as kernel density estimates, using an Epanechnikov kernel (Epanechnikov 1969) with a band-with of 0.2 mag.

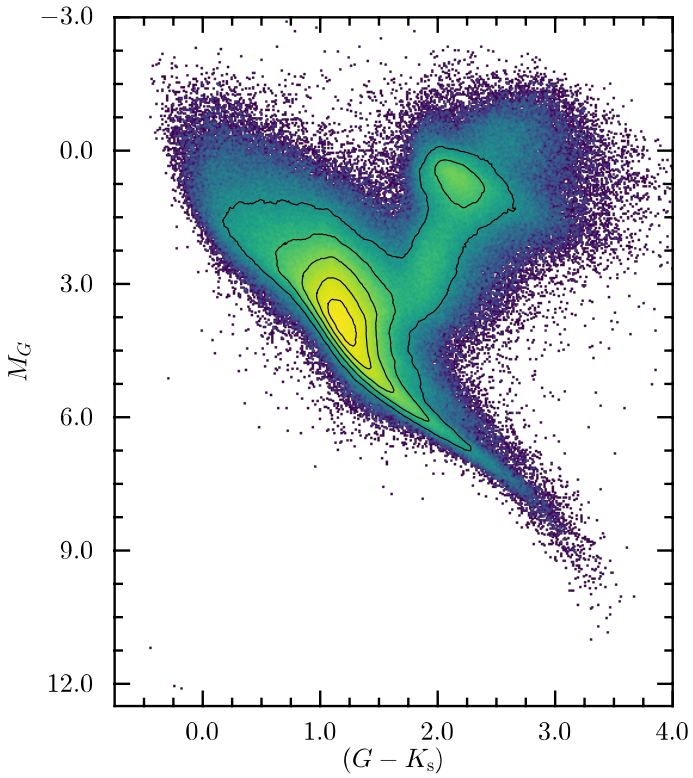

Fig. 5. Observational HR diagram for all stars in *Gaia* DR1 selected as explained in the text for which the $(G - K_s)$ colour index can be calculated from *Gaia* DR1 and the data in the 2MASS Point Source Catalogue. The visualisation is the same as in Fig. 3 with the contours enclosing 10%, 30%, 50%, 70%, and 90% of the data.

in the left two panels of Fig. 3 that have colours in the range $1.0 \leq (B-V) \leq 1.1$ (3174 stars), including both the clump stars around $M_G \sim 0.5$ and the main sequence dwarfs around $M_G \sim 6$, as well as a fraction of sub-giants (at $1 \lesssim M_G \lesssim 3$). The luminosity distributions for both the dwarfs and the clump giants are narrower for *Gaia* DR1 than for HIPPARCOS. For the dwarfs (defined as stars with $M_G > 4.5$) the robust scatter estimates for the width of the distribution of M_G (see Lindegren et al. 2016, for the definition of this quantity) are 0.32 for *Gaia* DR1 and 0.38 for HIPPARCOS. For the clump giants the numbers are sensitive to the range of M_G used to isolate the clump and whether that range is defined using the *Gaia* DR1 or HIPPARCOS luminosities. Using the broad selection $-0.5 \leq M_G(\text{HIPPARCOS}) \leq 1.5$ the robust scatter estimates are 0.37 for *Gaia* DR1 and 0.46 for HIPPARCOS. When isolating the clump giants using *Gaia* DR1 luminosities ($-0.2 \leq M_G(\textit{Gaia}\ \text{DR1}) \leq 1.2$) the robust scatter estimates are 0.30 for *Gaia* DR1 and 0.49 for HIPPARCOS. The detailed interpretation of the scatter in M_G for the red clump giants and how this relates to the parallax quality of *Gaia* DR1 and HIPPARCOS is complicated by the HIPPARCOS survey selection function, the filtering applied for *Gaia* DR1, the parallax systematics present in *Gaia* DR1 (see Sect. 6), and the biases introduced by the HIPPARCOS magnitude limit and the selection on relative parallax error. These effects lead to an incomplete and non-representative sample of red clump giants. A proper interpretation of the scatter in the luminosities (and of the mean observed luminosity) requires the modelling of the population of red clump giants and of the *Gaia* and HIPPARCOS survey properties, which we consider beyond the scope of the illustrations provided in this section.

The rightmost panel in Fig. 3 shows how in *Gaia* DR1 a larger volume is covered by relatively precise parallaxes; the overall width in colour of the upper main sequence and red clump is larger due to the larger extinction values probed, and the upper main sequence and giant branch are better populated. In numbers the median relative uncertainty on the HIPPARCOS parallax for the stars selected according to Eq. (2) is 0.1, while for the *Gaia* DR1 parallaxes it is 0.04.

In Fig. 5 we show the observational HR diagram for a much larger sample of stars from *Gaia* DR1 for which the $(G - K_s)$ colour index can be calculated from *Gaia* DR1 and the data in the 2MASS Point Source Catalogue (Skrutskie et al. 2006). The selection of the sources in this diagram is according to Eq. (2), where the limit on the HIPPARCOS relative parallax error does not apply and the limit on the standard uncertainty in the colour index now applies to $(G - K_s)$. In addition the 2MASS photometric quality flag was required to be equal to "A" for each of the J, H, and K_s magnitudes. The resulting sample contains 1 004 204 stars (there are 1 037 080 stars with $\varpi/\sigma_\varpi \geq 5$ in total in *Gaia* DR1). The sample covers a substantially larger volume, the median parallax being 2.9 mas, while 90 per cent of the stars have a parallax larger than 1.7 mas. The larger volume covered is evident from the large number of luminous stars in the HR diagram: 42 333 stars at $M_G < 2$ in the rightmost panel of Fig. 3, compared to 190 764 in Fig. 5. In addition the effect of extinction is now more prominently visible as a broadened upper main sequence and turn-off region, as well as in the elongation of the red clump. A hint of the binary sequence in parallel to the main sequence can be seen around $(G - K_s) \sim 2.2$ and $M_G \sim 6$. Note the three white dwarfs at $(G - K_s) < 0$ and $M_G > 11$; from the brightest to the faintest their 2MASS designations and *Gaia* source identifiers are 2MASS J21185627+5412413, 2MASS J16482562+5903228, 2MASS J19203492-0739597, and 2176116580055936512, 1431783457574556672, 4201781727042370176, respectively. This diagram is also an illustration of the use of pre-computed cross-match tables, linking *Gaia* DR1 and other large surveys, which are provided along with the data release (see Sect. 7 and Marrese et al. 2016).

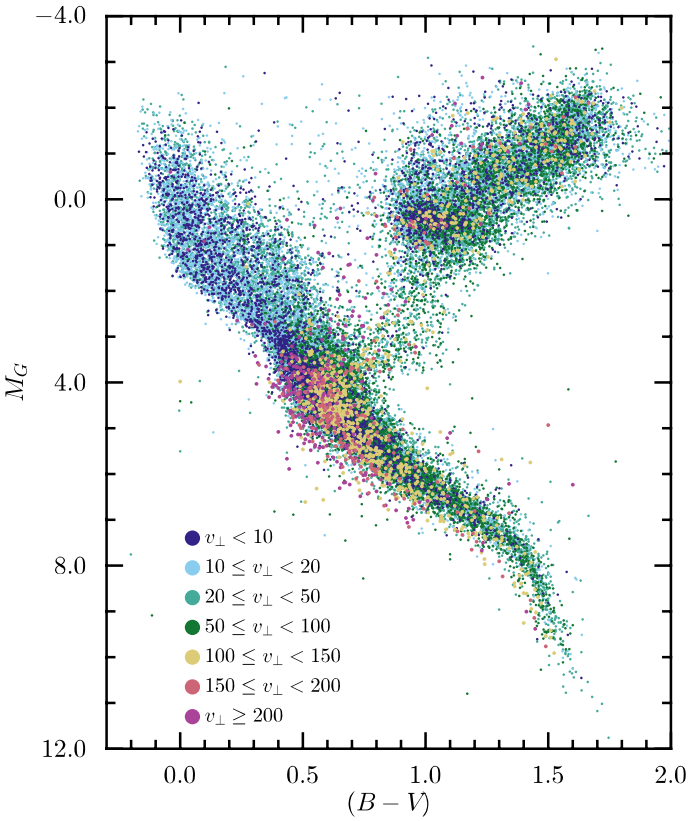

Fig. 6. Observational HR diagram showing where stars with specific values of the transverse velocity $v_\perp$ tend to occur. The colour coding of the points is according to tangential velocity interval, as indicated in the legend (in km s^{-1}).

An HR diagram can also be produced with the $(B - V)$ colour index. However, this requires the use of different sources for the colour index values. When we combined HIPPARCOS (ESA 1997; van Leeuwen 2007), *Tycho*-2 (Høg et al. 2000), and APASS (Henden & Munari 2014) a diagram containing only a third as many stars resulted. This reflects the lack of high quality all-sky optical photometry over the brightness range in between that covered by HIPPARCOS and modern digital sky surveys, such as the Sloan Digital Sky Survey (York et al. 2000), which usually only cover apparent magnitudes fainter than ∼15. This situation will be remedied with the second *Gaia* data release through the publication of the G_{BP} and G_{RP} magnitudes obtained from the integrated fluxes measured with the Blue and Red Photometers.

Finally, following Gould (2004), in Fig. 6 we show a version of the HR diagram which is colour coded according to the transverse velocity of the stars $v_\perp = \mu/\varpi \times 4.74\ldots$ (in km s^{-1}), where μ is the length of the proper motion vector of the star. The stars in this diagram were selected according to the criteria in Eq. (2) (without selecting on the HIPPARCOS relative parallax error), using the $(B - V)$ colour index as listed in the HIPPARCOS, *Tycho*-2, or APASS catalogues (in that order of preference), where the *Tycho*-2 colours were transformed to approximate Johnson colours according to: $(B - V)_J \approx 0.85(B - V)_T$ (ESA 1997, Sect. 1.3, Vol. 1). It was further demanded that $G \le 7.5$, or $\mu \ge 200$ mas yr^{-1}, or $\varpi \ge 10$ mas. The 41 136 stars in this diagram are represented by symbols which are colour coded by tangential velocity interval as indicated in the figure legend. This nicely illustrates the well known mix of stellar populations in a local sample (the median parallax for this sample being 10.7 mas, while 90 per cent of the stars have a parallax larger than 2.8 mas). At low velocities the young disk stars along the main sequence are outlined ($v_\perp < 50$ km s^{-1}). The turn-off region for the old disk is visible at 50 km s^{-1} $\le v_\perp <$ 100 km s^{-1}, while at higher velocities halo stars are visible, which along the main sequence are clearly shifted to the lower metallicity region.

5.3. Gaia DR1 proper motions

Given the different time spans that underlie the determinations of proper motions listed in the HIPPARCOS (Δepoch ∼ 3.5 yr), *Gaia* DR1 (Δepoch ∼ 24 yr), and *Tycho*-2 (Δepoch ∼ 90 yr) catalogues, it is interesting to look for sources with discrepancies between the proper motions listed in the three catalogues. The proper motion differences may point to the presence of non-modelled astrometric components (such as orbital motion in a binary), and thus to sources worthy of further investigation.

If this is attempted, very large discrepancies between *Gaia* DR1 and *Tycho*-2 proper motions may occur (of order 100–250 mas yr^{-1}), which seems surprising at first sight. We performed a close inspection of 39 such cases and examined proper motion solutions for these sources for which the *Tycho*-2 position was not used (these solutions are not published in *Gaia* DR1). In all cases there is close agreement (to within a few mas yr^{-1} in both coordinates) between the *Gaia*-only proper motion and the proper motion listed in *Gaia* DR1. The fact that *Gaia* measures the same proper motions over a 14 month time span as over the 24 yr time span used for the primary astrometric data set implies that the large discrepancies mentioned above are due to errors in the *Tycho*-2 proper motions. These errors are most likely caused by mismatches of the *Tycho* sources to old photographic catalogues, as was confirmed by inspecting the surroundings of a few sources among the 39 mentioned above.

The above example points to the high quality of the *Gaia* DR1 proper motions and serves as a warning not to over-interpret discrepancies between *Gaia* DR1 proper motions and those in existing proper motion catalogues.

5.4. Photometry of variable stars

Figure 7 shows two examples of phase-folded light curves from the Cepheids and RR Lyrae data set in *Gaia* DR1, one of a Cepheid and one of an RR Lyrae variable. Both curves highlight the quality of the *G*-band photometry in *Gaia* DR1. In the case of the Cepheid variable the error bars are comparable to or smaller than the symbol size, while for the RR Lyrae variable the uncertainties on the individual measurements are ∼0.02 mag. More light curves and an extensive description of the Cepheids and RR Lyrae variables in *Gaia* DR1 are presented in Clementini et al. (2016). The high cadence at which these stars were observed is not representative for the nominal *Gaia* mission, but reflects the special Ecliptic Pole Scanning Law used during the first weeks of the mission (Gaia Collaboration et al. 2016b).

5.5. Comment on the Pleiades cluster mean parallax

Since the publication of HIPPARCOS-derived trigonometric cluster parallaxes for the Pleiades (van Leeuwen 1999, 2009) there has been a discrepancy between the HIPPARCOS values and a number of other distance determinations derived with various methods. Figure 8 displays the set of existing measurements of either the parallax or the distance modulus of the cluster or of individual cluster members, all expressed as distances in parsecs.

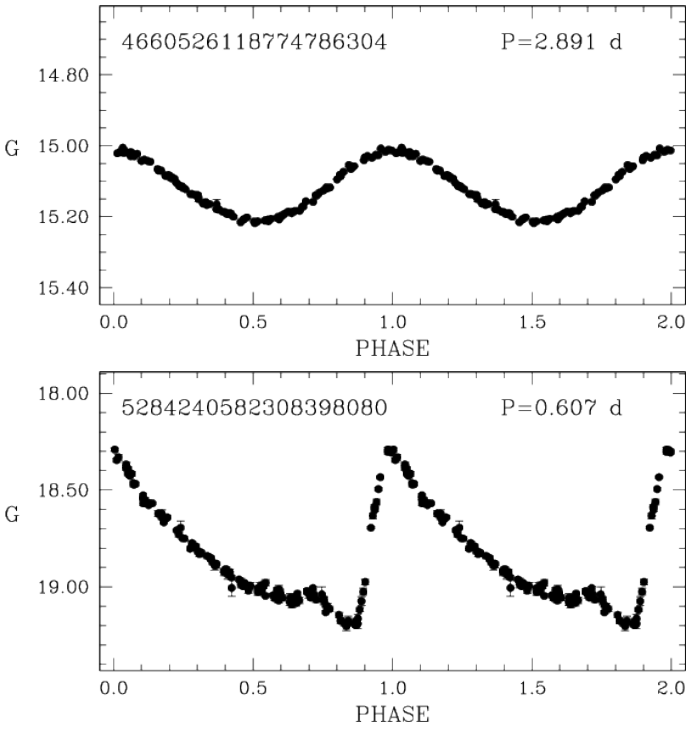

Fig. 7. Example light curves from the Cepheids and RR Lyrae data set in *Gaia* DR1. The *top panel* shows the light curve for a fundamental mode classical Cepheid in the Large Magellanic Cloud (period 2.891 days), while the *bottom panel* shows the light curve for a fundamental mode RR Lyrae star (RRab, period 0.607 days), also in the Large Magellanic Cloud.

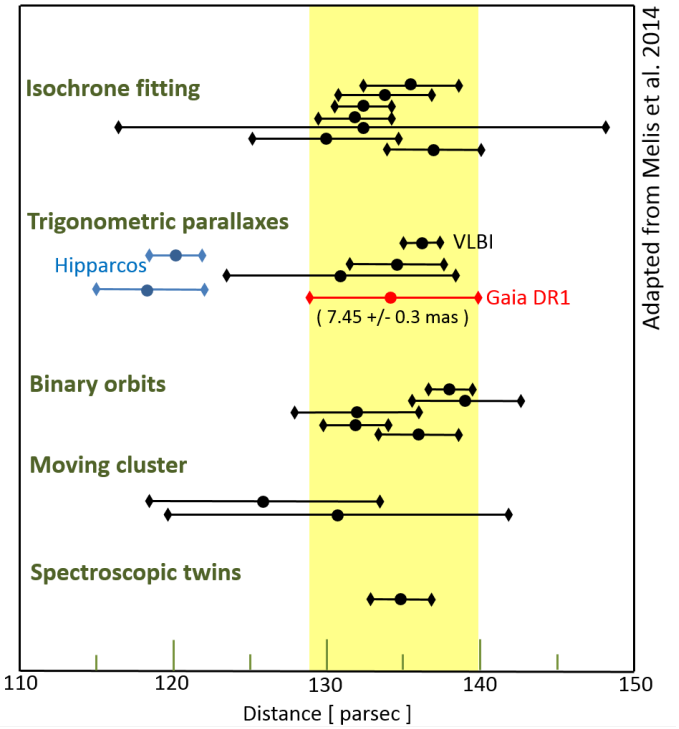

Fig. 8. Existing measurements of the parallax or distance modulus for the Pleiades cluster or individual cluster members, all expressed in parsecs. Figure adapted from Melis et al. (2014). The point indicated with "VLBI" is the distance corresponding to the parallax determined by Melis et al. (2014), while the point indicated with "Spectroscopic twins" is the distance corresponding to the parallax determined by Mädler et al. (2016). The references for the rest of the points can be found in Melis et al. (2014).

The *Gaia* DR1 adds another item to this set. It is indicated in Fig. 8 by the yellow shaded area.

A simplistic selection of Pleiades members can be done solely on the basis of the *Gaia* DR1 positions and proper motions by demanding that the selected stars lie within 5 degrees from the position $(\alpha, \delta) = (56.75°, 24.12°)$ and that the proper motions obey:

$$\left[(\mu_{\alpha*} - 20.5)^2 + (\mu_\delta + 45.5)^2\right]^{1/2} \leq 6 \text{ mas yr}^{-1} . \quad (3)$$

This leads to the selection of 164 stars from the *Gaia* DR1 primary astrometric data set. Figure 9 shows the histogram of the parallaxes of these 164 stars, which apart from a few outliers (field stars not belonging to the Pleiades) are well clustered in a peaked distribution. The median of this distribution is at $\varpi = 7.45$ mas, and the standard deviation (robustly estimated) of the distribution is 0.49 mas. If the observations were independent, this would lead to a standard uncertainty in the mean of $0.49/\sqrt{N} = 0.04$ mas. However, as described in the paper on the astrometric solution for *Gaia* DR1 (Lindegren et al. 2016) and in the paper on the validation of *Gaia* DR1 (Arenou et al. 2016), a not precisely known systematic uncertainty of the order of 0.3 mas must be added to the parallax uncertainties (see also Sect. 6). These systematic terms are correlated over small spatial scales, which means that the parallax uncertainties are not independent for the Pleiades members considered here, leading to no reduction of the uncertainties by averaging. Therefore the best estimate we can make at this time for the mean Pleiades parallax is 7.45 ± 0.3 mas, corresponding to a distance of about 134 ± 6 pc. This is indicated by the half-width of the yellow shaded area in Fig. 8.

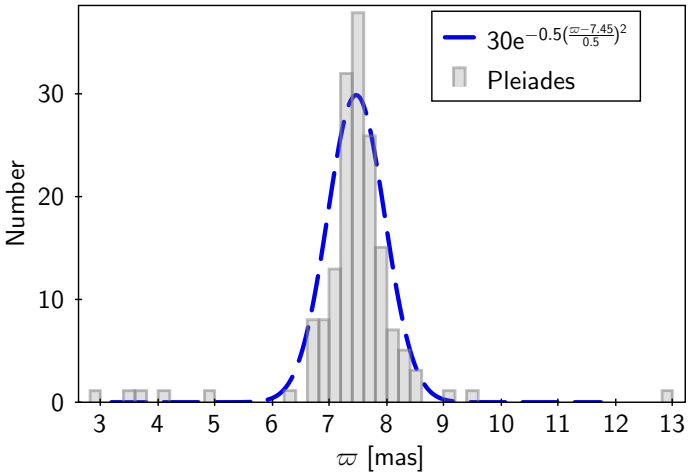

Fig. 9. Histogram of all *Gaia* DR1 parallaxes of proper motion selected Pleiades cluster members (using the proper motions of *Gaia* DR1 as the sole selection criterion). The over-plotted Gaussian distribution has a mean of 7.45 mas, a standard deviation of 0.5 mas and is normalised to a maximum value of 30 for comparison purposes.

We want to emphasise that, taking this systematic uncertainty into account, *Gaia* DR1 cannot be considered as giving a final and definite answer on the so-called Pleiades distance discrepancy. In particular an explanation for the discrepancy between *Gaia* DR1 and HIPPARCOS cannot be provided at this stage. A proper and more extensive analysis of the *Gaia* DR1 astrometry for nearby open clusters (including the Pleiades) is

presented in *Gaia* Collaboration et al. (2016c), with the results providing further arguments as to why the Pleiades distance estimated from *Gaia* DR1 parallaxes cannot be considered definitive. A conclusive answer to the question on the Pleiades distance – in the form of a sufficiently precise and systematically reliable trigonometric parallax for the cluster – can, however, be expected from future *Gaia* data releases (probably already *Gaia* DR2). What the present release definitely does is to make another significant addition to the accumulating information on the Pleiades distance which is summarised in Fig. 8.

6. Known limitations of *Gaia* DR1

Gaia DR1 represents a major advance in terms of the availability of high accuracy parallaxes and proper motions for the 2 million stars in the primary astrometric data set and in terms of accurate positions and homogeneous all-sky photometry for all sources out to the *Gaia* survey limit. Nevertheless the data release is based on an incomplete reduction of a limited amount of raw *Gaia* data and is thus of a very preliminary nature. We summarise the major shortcomings of *Gaia* DR1 in this section both to warn the users of the data and to enable a careful scientific exploitation of the *Gaia* DR1 data set. We stress however, that all the shortcomings listed below will be addressed in future *Gaia* data releases, with major improvements already expected for the second data release.

6.1. Data processing simplifications for Gaia DR1

We show in Fig. 10 in highly simplified form the DPAC data processing flow for the astrometric and photometric data reduction. The purpose of the diagram is to highlight the shortcomings in the data processing for *Gaia* DR1 compared to the intended data processing for future data releases (for simplicity many processing steps are left out, including the processing of the RVS data and the derivation of higher level results, such as source astrophysical parameters). The steps that should be taken during the processing are:

1. From the raw data derive (initial) calibrations of the *Gaia* PSF, the CCD bias, the astrophysical and stray light induced background flux in the image, and the parameters describing the charge transfer inefficiency (CTI) effects in the CCDs.
2. Use the calibrations to determine from the raw CCD-level measurements both the source flux and the source location within the observation window.
3. Use the spacecraft attitude to create the source list, by assigning observations (focal plane transits) to existing sources or by creating new sources if needed.
4. Process the image fluxes to derive calibrated G-band photometry and process the BP/RP data to derive the source colours. Process the image locations in order to derive the astrometric source parameters, the attitude model for the *Gaia* spacecraft, and the geometric instrument calibrations.
5. Introduce the known source locations on the sky, the geometric instrument calibrations, the attitude model, and the source colours into step 1 above and improve the accuracy of the calibrations.
6. Repeat steps 2 and 3 using the improved astrometry and calibrations from step 5. Subsequently repeat step 4 using the improved image locations and fluxes.
7. Iterate the above steps, including progressively more data, until convergence on the final astrometric and photometric results at their ultimately attainable accuracy.

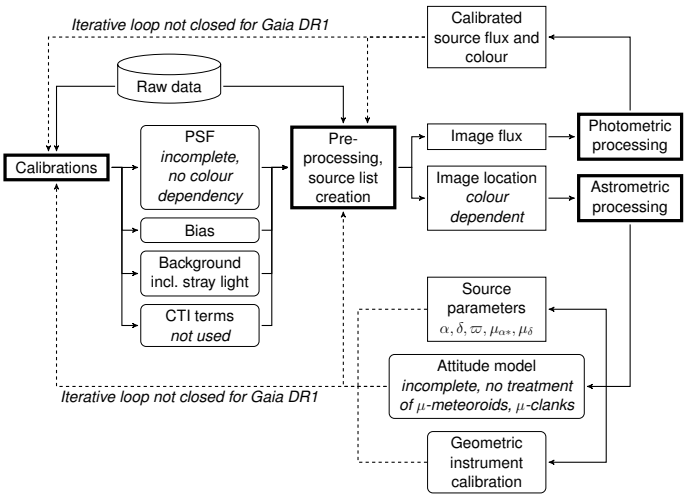

Fig. 10. The DPAC data processing flow as used for *Gaia* DR1 in schematic and simplified form. Thick lined boxes show processing steps, rounded boxes represent calibrations derived during the processing, while thin-lined boxes show processing outputs. The solid lines indicate the processing flow as realised for *Gaia* DR1, while the dashed lines indicate processing flows that were not implemented for *Gaia* DR1. The remarks in italics highlight important shortcomings in the *Gaia* DR1 processing.

As illustrated in Fig. 10 steps 5–7 above were not carried out during the processing for *Gaia* DR1, which means that the inputs for the astrometric and photometric processing are limited in quality due to the use of immature calibrations, in particular an incomplete PSF model which does not account for source colour effects on the detailed image shape, or for PSF variations across the focal plane and in time. The source locations within the images and the astrometry derived from those will be strongly affected by systematics related to source colour (see Lindegren et al. 2016, appendix C). Systematic effects related to the PSF model can also be expected in the G-band photometry derived from the image fluxes. A further limitation to the quality of *Gaia* DR1 astrometry, indicated in Fig. 10, is that the attitude modelling within the astrometric solution is incomplete. No treatment of micro-meteoroid hits or micro-clanks was included (except for the exclusion of the data from short time intervals affected by large hits) leading to attitude modelling errors which in turn will limit the astrometric accuracy that can be attained (see Lindegren et al. 2016, in particular appendix D). The treatment of CTI effects was not included in *Gaia* DR1, which is justified given the present low levels of radiation damage to the *Gaia* CCDs (Crowley et al. 2016a).

We stress that the above description of the data processing for *Gaia* DR1 is mainly illustrative and not intended as a complete description of all the simplifications that were introduced to enable a timely first *Gaia* data release. For details on the actual processing for *Gaia* DR1 refer to Fabricius et al. (2016) (pre-processing and source list creation), van Leeuwen et al. (2016), Carrasco et al. (2016), Riello et al. (2016) (photometric processing), Eyer et al. (2016) (variable star processing), and Lindegren et al. (2016) (astrometric processing). In particular the latter paper contains an extensive description of the known problems introduced by the preliminary astrometric processing.

In the following subsections we summarise the most prominent issues with *Gaia* DR1 which should be taken into consideration when using the data for scientific analyses. These concern catalogue completeness, and systematics in the astrometric

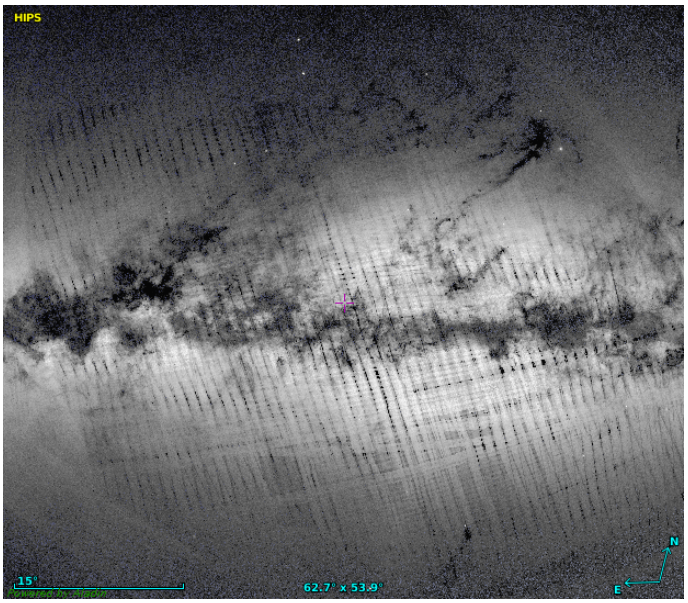

Fig. 11. *Gaia* DR1 source density distribution on the sky in the direction of the Milky Way bulge region. Note the prominent "striping" and the gaps in the source distribution.

and photometric results which were revealed during the validation of the DPAC outputs produced for *Gaia* DR1. Much more detail on the validation of *Gaia* DR1 can be found in Lindegren et al. (2016), Evans et al. (2016), Eyer et al. (2016), Arenou et al. (2016).

6.2. Gaia DR1 source list and completeness

The *Gaia* DR1 celestial source density distribution shown in Fig. 2 contains a number of clearly non-astronomical artefacts, which is illustrated in more detail in Fig. 11 for the Milky Way bulge region. In particular away from the Milky Way plane, but also across the Bulge region, Fig. 2 shows obvious source under-densities as well as *apparent* over-densities, where the latter surround the regions (along the ecliptic) dominated by the former.

The patterns in Fig. 2 are related to the *Gaia* scanning law (cf. Gaia Collaboration et al. 2016b) and are caused by the source filtering applied for *Gaia* DR1. The areas around the ecliptic are inherently observed less often due to the characteristics of the scanning law, and in particular have been rather poorly observed over the first 14 months of the mission (covering *Gaia* DR1), both in terms of the number of visits and the coverage in scanning direction. This results in the sources in the less well covered areas having a larger probability of being filtered out, which gives the regions in between (with far fewer sources filtered out) the appearance of containing more sources. Hence Fig. 2 shows primarily a deficit of sources in the less well observed regions of the sky.

This is illustrated in more detail for the Milky Way bulge region in Fig. 11 The pattern of dark stripes, with a clear lack of sources, is again related to the *Gaia* scanning law. The bulge lies in the ecliptic region and thus suffers from poor scan law coverage in *Gaia* DR1. In combination with the filtering on the astrometric solution quality prior to *Gaia* DR1 publication this can even lead to areas where sources are entirely missing. This is illustrated in Fig. 12, which shows the circle on the sky around $(\alpha, \delta) = (266^\circ, -18.5^\circ)$ with a 0.5 degree radius. The top panel shows the distribution of the 268 435 sources in this area. The

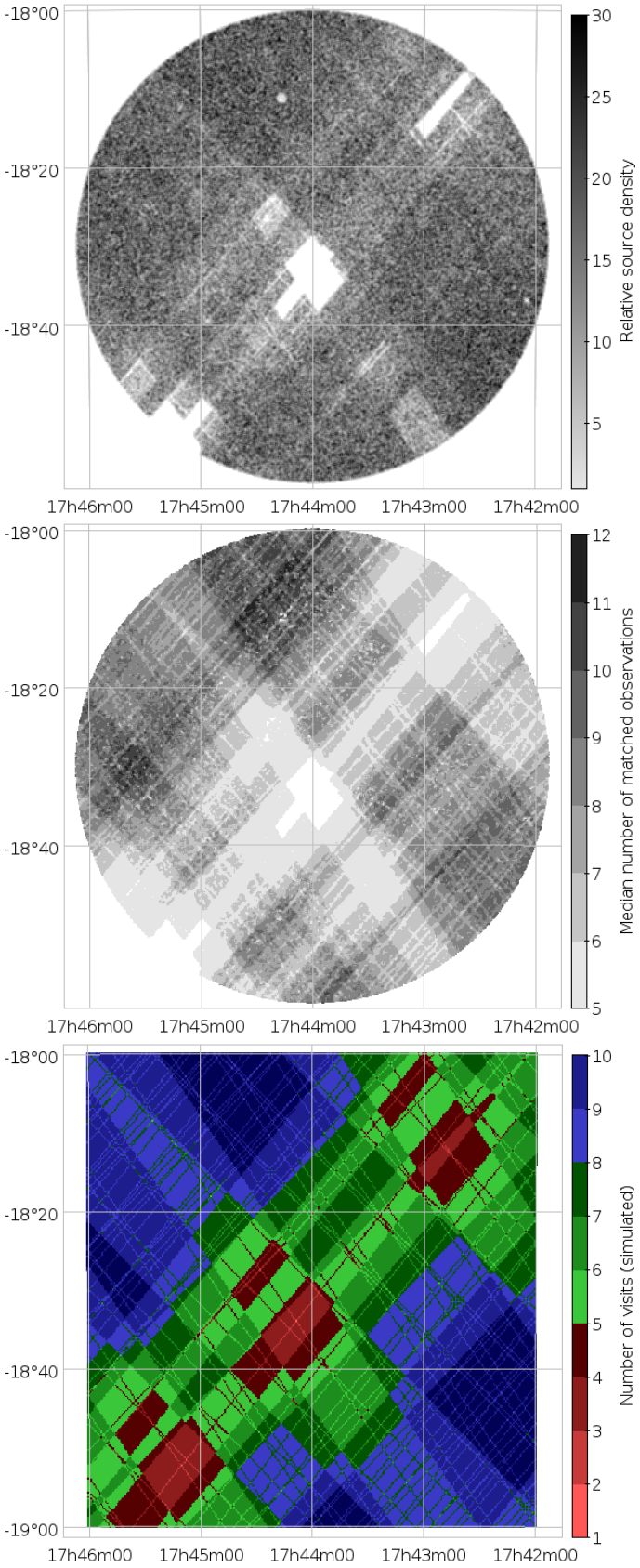

Fig. 12. Illustration of how the combination of scan law coverage and data filtering leads to gaps in the *Gaia* DR1 source distribution. The *top panel* shows the source density in the area of 0.5 degree radius around $(\alpha, \delta) = (266^\circ, -18.5^\circ)$. The *middle panel* shows the median number of observations (i.e. focal plane transits) that were matched to each source. The *bottom panel* shows the predicted number of visits by *Gaia* according to the nominal scanning law.

distribution shows the striping pattern and also contains very thin strips where fewer sources than the average are found. Most prominent, however, are three large gaps where no sources occur. The middle panel shows the median number of observations matched to each source in this region and there the pattern is even richer. We note that the minimum number of observations is five (as demanded by the filtering applied, see Sect. 4), suggesting that the gaps are related to the number of times a particular coordinate on the sky was visited by *Gaia*. This is confirmed in the bottom panel which shows a simulation of the expected number of visits corresponding to the scanning law as executed between September 2014 and September 2015. This time period does not cover the ecliptic pole scanning phase, but during that phase this region on the sky was not observed. The gaps in the source distribution correspond to the areas in the simulation where fewer than five visits by *Gaia* occur, which thus explains the gaps as being due to the filtering applied for *Gaia* DR1. In addition the simulation shows the same very thin strips where *Gaia* has collected fewer observations than the maximum of 12 occurring in this area on the sky. Whenever few observations are collected there is a good chance that the source gets filtered out if focal plane transits from particular visits by *Gaia* are discarded for other reasons and thus the total number of observations drops below five. Although the simulated scan law coverage very much resembles the pattern in the number of matched observations, there are differences in detail because the actually executed scanning law differs somewhat from the nominal scanning law used in the simulation.

The striping pattern seen over the bulge region in Fig. 11 can thus be explained as a consequence of the *Gaia* scan law coverage over the first 14 months of the mission combined with the filtering applied to the astrometric results before including them in *Gaia* DR1. Although the striping and gaps are most prominently visible in the bulge region this pattern also occurs in other parts of the sky in the ecliptic region, notably along the Milky Way plane in the anti-centre direction. In these areas the step changes in the number of observations collected by *Gaia* combined with the filtering has in some unlucky cases led to one half of an open cluster partly missing from the catalogue.

Further remarks on the catalogue completeness are the following:

- Many bright stars at $G \lesssim 7$ are missing from *Gaia* DR1 as the corresponding measurements cannot yet be treated routinely by the DPAC. The images are heavily saturated and the instrument configuration (TDI gate setting used) is difficult to calibrate due to the sparsity of bright sources on the sky.
- High proper motion stars ($\mu > 3.5$ arcsec yr^{-1}) are missing from the catalogue due to a technical issue in the construction of the IGSL (cf. Lindegren et al. 2016).
- As mentioned in Sect. 4 extremely blue and red sources are missing from *Gaia* DR1 which, for example, affects the completeness of the white dwarf population in *Gaia* DR1 and that of sources in extincted regions (cf. Arenou et al. 2016).
- In dense areas on the sky (with source densities above a few hundred thousand per square degree) the crowding of sources will lead to the truncation of the observation windows for some stars when they overlap with the window of another star. These truncated windows have not been used in the data processing for *Gaia* DR1. This means that in dense areas the average number of transits used per source will be smaller (especially for fainter sources), which in combination with the filtering on the number of observations and the astrometric or photometric solution quality means these sources may have been removed from *Gaia* DR1.
- The survey completeness is also affected by the way the data is treated on board *Gaia*, meaning both the detection of sources and the assignment of observation windows. The details are provided in Gaia Collaboration et al. (2016b). We note here that in very dense areas (above ∼400 000 stars per square degree) the effective magnitude limit of the *Gaia* survey may be brighter by up to several magnitudes, with data for faint sources being collected for a reduced number of focal plane transits.
- An examination of double stars from the Washington Visual Double Star Catalog (Mason et al. 2001) contained in *Gaia* DR1 shows that below about 4 arcsec there is a notable decrease in the completeness of the detection of the secondaries, which is related to the above mentioned limitations in crowded regions (Arenou et al. 2016). The implication of this finding and the previous two items is that the effective angular resolution on the sky of *Gaia* DR1, in particular in dense areas, is not yet at the levels expected for the 1.5 m *Gaia* telescope mirrors (which should lead to an angular resolution comparable to that of the *Hubble* Space Telescope).

The limitations to the *Gaia* DR1 source list described above lead to a catalogue which is not complete in any sense and for which the faint magnitude limit is ill-defined and dependent on celestial position. No attempt was made to derive a detailed completeness function. Hence when using the catalogue for scientific analyses, care needs to be taken with the interpretation of source distributions both on the sky and in apparent magnitude.

6.3. Known problems in the Gaia DR1 photometry

Although the G-band fluxes and magnitudes provided with *Gaia* DR1 have standard uncertainties as good as a few per cent in magnitude at the survey limit and down to the milli-magnitude level at the bright end, there are nevertheless limitations inherent to this first *Gaia* data release. The G-band fluxes were derived as part of the image parameter determination in the initial data treatment (see Sect. 6.1 above and Fabricius et al. 2016) and thus suffer from the lack of an accurate PSF model. In addition at the bright end ($G < 12$) the calibrations of the photometry are complicated by the use of TDI gates, while over the range $G = 12$–17 the effects of different observation window sizes make the calibration more complex. The result is that for the brightest, $G < 12$, stars the photometric accuracy is estimated to currently be limited to a calibration floor of ∼3 mmag for the individual CCD transits, (van Leeuwen et al. 2016; Evans et al. 2016). The quoted standard uncertainties on the mean G-band magnitudes at the bright end can vary by an order of magnitude (caused by poorly calibrated transitions from one TDI gate setting to another). Over the range $G = 12-17$ the distribution of photometric standard errors as a function of magnitude shows two bumps at $G \sim 13$ and $G \sim 16$ which are related to the transition from one observation window type to another (van Leeuwen et al. 2016). An examination of the scatter in repeated photometric measurements for well-observed sources indicates that the quoted standard uncertainties on the G-band photometry are largely realistic as indicators of the photometric precision (see Evans et al. 2016, for details), however unaccounted for systematic errors cannot be excluded. Potential systematic errors in the photometry are discussed in Evans et al. (2016) and Arenou et al. (2016). There is a small fraction of sources for which the mean value of G is clearly wrong. These are sources

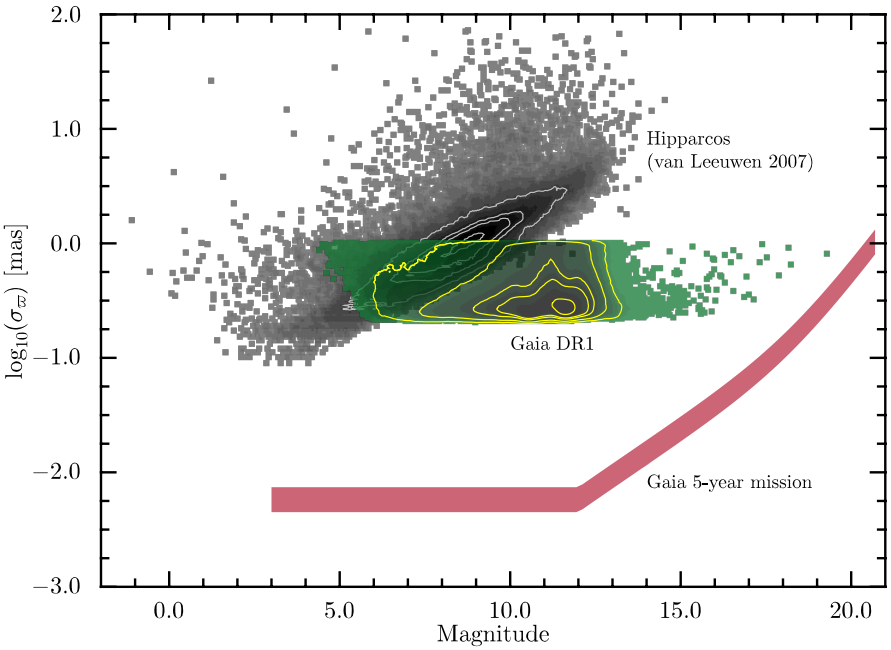

Fig. 13. Parallax standard uncertainties as a function of magnitude for HIPPARCOS (van Leeuwen 2007) and the primary astrometric data set in *Gaia* DR1, compared to the predicted 5-yr *Gaia* mission parallax standard uncertainties. The band for the 5-yr mission predictions indicates the expected variation as a function of celestial position. The colour coding for the HIPPARCOS and *Gaia* DR1 parallax uncertainty distributions indicates increasing numbers of sources from light to dark colours (logarithmic scale). The contours enclose 10, 50, 68.3, and 90 per cent of the data in the case of HIPPARCOS, while for *Gaia* DR1 they enclose 10, 50, 68.3, 95.4, and 99.7 per cent of the data.

with magnitudes well beyond the *Gaia* survey limit of $G = 20.7$ and also at brighter magnitudes such errors occur as evidenced by the presence of a small number of *Tycho*-2 sources with magnitudes up to $G \sim 19$ (cf. Fig. 13), although it should be noted that a number of these sources may well be variables with large brightness excursions, leading to faint magnitudes at the *Gaia* DR1 observation epoch.

6.4. Known problems in the Gaia DR1 astrometry

The data processing shortcuts and simplifications discussed in Sect. 6.1 have introduced a number of known weaknesses in the astrometric solution for *Gaia* DR1, which are described and explained extensively in Lindegren et al. (2016). Here we highlight the weaknesses most directly relevant to the scientific exploitation of the *Gaia* DR1 data.

Source modelling All sources were treated as single stars without taking their radial velocity into account. Hence any astrometric effects due to the orbital motion in binaries or due to perspective acceleration were ignored. In addition for resolved binaries the positions used to derive the mean proper motion over the time period between the HIPPARCOS/*Tycho* (around J1991.25) and the *Gaia* DR1 (J2015.0) epochs may be inconsistent (cf. Lindegren et al. 2016). The *Gaia* DR1 catalogue does provide the so-called excess source noise, which is meant to represent the astrometric modelling errors for a specific source, and thus could in principle be used to identify candidate astrometric binaries or otherwise problematic sources. However in *Gaia* DR1 all sources have significant excess source noise because currently unmodelled attitude and calibration errors are partly "absorbed" in this quantity (see Lindegren et al. 2016, for more details). The level at which the excess source noise is indicative of a source being different from a single star should thus be calibrated against a sample of known non-single star sources in *Gaia* DR1 before it can be used in scientific analyses.

Periodic basic angle variations As described in Gaia Collaboration et al. (2016b), a number of issues affecting the performance of the *Gaia* instruments came to light during the commissioning period. The most relevant issue for the astrometric quality of *Gaia* DR1 is the periodic variation of the basic angle between the two telescopes of *Gaia*. This angle enters into all the measurements of angular separations between sources on the sky and its value should either be stable or its variations known at the level of ∼1 μas. The actual basic angle variations, measured both through the on board metrology system and from the daily astrometric solution carried out as part of the DPAC First-Look analysis (see Fabricius et al. 2016), have a component which varies periodically with the satellite spin period and with a significant amplitude of roughly 1 mas. The harmonic component that varies as the cosine of the spacecraft heliotropic spin phase cannot be distinguished from a zero-point offset in the parallaxes, making the calibrations of the basic angle variations an essential component of the success of *Gaia* (for more detail see Michalik & Lindegren 2016). For *Gaia* DR1 the corrections for the basic angle variations were done by adopting the variations as measured by the on-board metrology system. At the accuracy level of *Gaia* DR1 this is sufficient. However Lindegren et al. (2016) do conclude that a global parallax zero point offset of ±0.1 mas may be present, which is confirmed by the zero-point offset of about −0.04 mas found during the validation of *Gaia* DR1 (Arenou et al. 2016). For future data releases the basic angle variations will largely be determined as calibration parameters within the astrometric solution (cf. Lindegren et al. 2016) with the aim to fully account for the variations.

Strongly correlated astrometric parameters Figure 7 in Lindegren et al. (2016) presents a statistical overview of the standard uncertainties and the correlations between the astrometric parameters of each source in the primary astrometric data set. In *Gaia* DR1 the correlation levels are high, reaching median values near −1 or +1 over large regions of the sky. It is thus very important to make use of the full covariance matrix when taking the standard uncertainties on (subsets and linear combinations of) the astrometric parameters into account in any scientific analysis of the data. The correlations will decrease in future data

releases as the number of observations per source and the scan direction diversity increase.

Spatially correlated systematics Several of the weaknesses in the astrometric solution identified in Lindegren et al. (2016) will lead to systematic errors that are colour dependent and spatially correlated over areas on the sky that may extend up to tens of degrees. One important contributor to these correlations is the incomplete modelling of the spacecraft attitude, which is extensively described in appendix D.3 of Lindegren et al. (2016). Special astrometric validation solutions indeed point to the presence of spatially correlated and colour-dependent systematics of ±0.2 mas. The global validation of the astrometric results confirms the presence of spatial variations of the parallax zero-point (see Arenou et al. 2016). Over large spatial scales the parallax zero-point variations reach an amplitude of ∼0.3 mas, while over a few smaller areas (∼2 degree radius) much larger parallaxes biases may occur of up to ±1 mas. The recommendation is to consider the quoted uncertainties on the parallaxes as $\varpi \pm \sigma_\varpi$ (random) ± 0.3 mas (systematic). Furthermore averaging parallaxes over small regions of the sky will not reduce the uncertainty on the mean below the 0.3 mas level. Similar studies into proper motion biases are not possible due to the limited accuracy of ground-based proper motion catalogues.

Finally, we illustrate graphically the preliminary nature of the *Gaia* DR1 astrometry in Fig. 13. It shows the distribution of parallax standard uncertainties as a function of magnitude for HIPPARCOS (van Leeuwen 2007) and *Gaia* DR1, and the expected parallax standard uncertainties achievable after a 5-yr *Gaia* mission (as provided in Gaia Collaboration et al. 2016b). Note how in contrast to HIPPARCOS the *Gaia* DR1 parallax standard uncertainties do not decrease with increasing source brightness but stay at the same level. This is partly related to the gating strategy for bright ($G < 12$) sources which prevents significant gains in signal to noise ratio, but the uncertainty levels are much more than a factor of 2 away from the 5-year mission uncertainty floor at the bright end (where the factor of 2 is the gain in signal to noise going from 14 to 60 months of observations). This indicates that the parallax uncertainties are dominated by calibration errors at this stage, the calibration floor being ∼0.2 mas. The second important point in this figure is that the expected 5-yr parallax standard uncertainties are much better than what can be achieved for *Gaia* DR1, with the current parallax standard uncertainty levels being comparable to the standard uncertainty levels that can ultimately be achieved at the *Gaia* survey limit.

7. *Gaia* DR1 access facilities

Access to the data contained in *Gaia* DR1 is provided through various channels. The main access point is the ESA *Gaia* Archive, which can be accessed through `http://archives.esac.esa.int/gaia/`. The archive provides access to the data through simple query forms but also allows the submission of sophisticated data base queries in the Astronomical Data Query Language (Osuna et al. 2008). The electronic tables comprising *Gaia* DR1 contain descriptions of each data field which can be inspected online. The *Gaia* archive is Virtual Observatory (`http://www.ivoa.net/`) compatible and also allows for access through the Table Access Protocol (Dowler et al. 2010). More extensive documentation, providing more detail on the data processing than is possible to include in peer-reviewed papers, is available from the archive in various electronic formats. Further tools provided are a visualisation application, graphics with statistical overviews of the data, an online help system, and the means to upload user generated tables which can be combined with *Gaia* data and shared with other users of the *Gaia* archive. More details on the data access facilities are provided in Salgado & et al. (2016).

As part of the archive services pre-computed cross-match tables linking *Gaia* DR1 to other large surveys are provided to facilitate the analysis of combined data sets. The details on how these cross-match tables were computed are provided in Marrese et al. (2016).

Finally, the *Gaia* DR1 data is also made available through a number of partner and affiliated data centres located in Europe, the United States, South Africa, and Japan. These data centres do not necessarily hold all the data contained in the *Gaia* archive and may layer their own access and analysis facilities on top of the *Gaia* data.

8. Conclusions

Less than three years after the launch of *Gaia* we present the first *Gaia* data release, where the use of positional information from the HIPPARCOS and *Tycho*-2 catalogues allowed the derivation of positions, parallaxes, and proper motions for about 2 million sources from the first 14 months of observations. This represents a data release that was not foreseen in the original *Gaia* mission planning and presents the astronomical community with advanced access to a large set of parallaxes and proper motions for sources to magnitude 11.5, at precisions substantially better than previously available. The release contains the positions and the mean G-band magnitudes for an additional 1141 million sources to the *Gaia* survey limit at $G \approx 20.7$, as well as the light curves for a sample of about three thousand variable stars.

The typical uncertainty for the position and parallaxes for sources in the primary astrometric data set is about 0.3 mas, and about 1 mas yr^{-1} for the proper motions. We stress again that a systematic component of ∼0.3 mas should be added to the parallax uncertainties and that averaging parallaxes over small regions on the sky will not lead to a gain in precision. For the subset of HIPPARCOS stars in the primary astrometric data set the proper motions are much more precise, at about 0.06 mas yr^{-1} (albeit with a systematic uncertainty at the same level). The positions of the sources in the secondary astrometric data set are typically known to ∼10 mas. The positions and proper motions are given in a reference frame that is aligned with the International Celestial Reference Frame (ICRF) to better than 0.1 mas at epoch J2015.0, and non-rotating with respect to ICRF to within 0.03 mas yr^{-1}.

The photometric data comprises the mean *Gaia* G-band magnitudes for all the sources contained in *Gaia* DR1, with uncertainties ranging from a few milli-magnitudes at the bright end to ∼0.03 mag at the survey limit (although systematic errors cannot be excluded), as well as light curves for 599 Cepheids and 2595 RR Lyrae variables observed at high cadence around the south ecliptic pole.

We have illustrated the scientific quality of the *Gaia* DR1 and have also pointed out the substantial shortcomings and the preliminary nature of this first *Gaia* data release. When using the data presented here the warnings given in Sect. 6 should be considered carefully. However, we are confident of the overall quality of the data, which represents a major advance in terms of available precise positions, parallaxes, proper motions, and homogeneous all-sky photometry. In addition, the scientific exploitation of the data at this early stage will surely improve the quality of future *Gaia* data releases.

We note in closing that all of the shortcomings listed in this and the accompanying *Gaia* DR1 papers will be addressed in future *Gaia* data releases with very substantial improvements already expected for *Gaia* DR2.

Acknowledgements. This work has made use of results from the European Space Agency (ESA) space mission *Gaia*, the data from which were processed by the *Gaia* Data Processing and Analysis Consortium (DPAC). Funding for the DPAC has been provided by national institutions, in particular the institutions participating in the *Gaia* Multilateral Agreement. The *Gaia* mission website is `http://www.cosmos.esa.int/gaia`. The authors are current or past members of the ESA *Gaia* mission team and of the *Gaia* DPAC. This work has received financial supported from the Algerian Centre de Recherche en Astronomie, Astrophysique et Géophysique of Bouzareah Observatory; the Austrian FWF Hertha Firnberg Programme through grants T359, P20046, and P23737; the BELgian federal Science Policy Office (BELSPO) through various PROgramme de Développement d'Expériences scientifiques (PRODEX) grants; the Brazil-France exchange programmes FAPESP-COFECUB and CAPES-COFECUB; the Chinese National Science Foundation through grant NSFC 11573054; the Czech-Republic Ministry of Education, Youth, and Sports through grant L.G. 15010; the Danish Ministry of Science; the Estonian Ministry of Education and Research through grant IUT40-1; the European Commission's Sixth Framework Programme through the European Leadership in Space Astrometry (ELSA) Marie Curie Research Training Network (MRTN-CT-2006-033481), through Marie Curie project PIOF-GA-2009-255267 (SAS-RRL), and through a Marie Curie Transfer-of-Knowledge (ToK) fellowship (MTKD-CT-2004-014188); the European Commission's Seventh Framework Programme through grant FP7-606740 (FP7-SPACE-2013-1) for the *Gaia* European Network for Improved data User Services (GENIUS) and through grant 264895 for the *Gaia* Research for European Astronomy Training (GREAT-ITN) network; the European Research Council (ERC) through grant 320360 and through the European Union's Horizon 2020 research and innovation programme through grant agreement 670519 (Mixing and Angular Momentum tranSport of massIvE stars – MAMSIE); the European Science Foundation (ESF), in the framework of the *Gaia* Research for European Astronomy Training Research Network Programme (GREAT-ESF); the European Space Agency in the framework of the *Gaia* project; the European Space Agency Plan for European Cooperating States (PECS) programme through grants for Slovenia; the Czech Space Office through ESA PECS contract 98058; the Academy of Finland; the Magnus Ehrnrooth Foundation; the French Centre National de la Recherche Scientifique (CNRS) through action "Défi MASTODONS"; the French Centre National d'Etudes Spatiales (CNES); the French L'Agence Nationale de la Recherche (ANR) "investissements d'avenir" Initiatives D'EXcellence (IDEX) programme PSL$*$ through grant ANR-10-IDEX-0001-02; the Région Aquitaine; the Université de Bordeaux; the French Utinam Institute of the Université de Franche-Comté, supported by the Région de Franche-Comté and the Institut des Sciences de l'Univers (INSU); the German Aerospace Agency (Deutsches Zentrum für Luft- und Raumfahrt e.V., DLR) through grants 50QG0501, 50QG0601, 50QG0602, 50QG0701, 50QG0901, 50QG1001, 50QG1101, 50QG140, 50QG1401, 50QG1402, and 50QG1404; the Hungarian Academy of Sciences through Lendület Programme LP2014-17; the Hungarian National Research, Development, and Innovation Office through grants NKFIH K-115709 and PD-116175; the Israel Ministry of Science and Technology through grant 3-9082; the Agenzia Spaziale Italiana (ASI) through grants I/037/08/0, I/058/10/0, 2014-025-R.0, and 2014-025-R.1.2015 to INAF and contracts I/008/10/0 and 2013/030/I.0 to ALTEC S.p.A.; the Italian Istituto Nazionale di Astrofisica (INAF); the Netherlands Organisation for Scientific Research (NWO) through grant NWO-M-614.061.414 and through a VICI grant to A. Helmi; the Netherlands Research School for Astronomy (NOVA); the Polish National Science Centre through HARMONIA grant 2015/18/M/ST9/00544; the Portugese Fundação para a Ciência e a Tecnologia (FCT) through grants PTDC/CTE-SPA/118692/2010, PDCTE/CTE-AST/81711/2003, and SFRH/BPD/74697/2010; the Strategic Programmes PEst-OE/AMB/UI4006/2011 for SIM, UID/FIS/00099/2013 for CENTRA, and UID/EEA/00066/2013 for UNINOVA; the Slovenian Research Agency; the Spanish Ministry of Economy MINECO-FEDER through grants AyA2014-55216, AyA2011-24052, ESP2013-48318-C2-R, and ESP2014-55996-C2-R and MDM-2014-0369 of ICCUB (Unidad de Excelencia 'María de Maeztu); the Swedish National Space Board (SNSB/Rymdstyrelsen); the Swiss State Secretariat for Education, Research, and Innovation through the ESA PRODEX programme, the Mesures d'Accompagnement, and the Activités Nationales Complémentaires; the Swiss National Science Foundation, including an Early Postdoc.Mobility fellowship; the United Kingdom Rutherford Appleton Laboratory; the United Kingdom Science and Technology Facilities Council (STFC) through grants PP/C506756/1 and ST/I00047X/1; and the United Kingdom Space Agency (UKSA) through grants ST/K000578/1 and ST/N000978/1. We acknowledge the valuable advice provided by Vincenzo Innocente (CERN) during two pre-launch reviews of DPAC. This research has made use of the Set of Identifications, Measurements, and Bibliography for Astronomical Data (Wenger et al. 2000) and of the "Aladin sky atlas' (Bonnarel et al. 2000; Boch & Fernique 2014), which are developed and operated at Centre de Données astronomiques de Strasbourg (CDS), France. Some of the figures in this paper were made with TOPCAT (`http://www.starlink.ac.uk/topcat/`) or through the use of the STIL library (`http://www.starlink.ac.uk/stil`). This research made use of the AAVSO Photometric All-Sky Survey (APASS, `https://www.aavso.org/apass`), funded by the Robert Martin Ayers Sciences Fund. This publication made use of data products from the Two Micron All Sky Survey, which is a joint project of the University of Massachusetts and the Infrared Processing and Analysis Center/California Institute of Technology, funded by the National Aeronautics and Space Administration and the National Science Foundation. We thank the anonymous referee for suggestions that helped improve this paper.

References

Arenou, F., Luri, X., Babusiaux, C., et al. 2016, A&A, this volume
Boch, T., & Fernique, P. 2014, in Astronomical Data Analysis Software and Systems XXIII, eds. N. Manset, & P. Forshay, ASP Conf. Ser., 485, 277
Bonnarel, F., Fernique, P., Bienaymé, O., et al. 2000, A&AS, 143, 33
Campbell, H. C., Marsh, T. R., Fraser, M., et al. 2015, MNRAS, 452, 1060
Carrasco, J. M., Evans, D. W., Montegriffo, P., et al. 2016, A&A, this volume
Clementini, G., Ripepi, V., Leccia, S., et al. 2016, A&A, this volume
Cropper, M., & Katz, D. 2011, in EAS PS, 45, 181
Crowley, C., Abreu, A., Kohley, R., Prod'homme, T., & Beaufort, T. 2016a, ArXiv e-prints [arXiv:1608.01476]
Crowley, C., Kohley, R., Hambly, N. C., et al. 2016b, A&A, this volume
Dowler, P., Rixon, G., & Tody, D. 2010, Table Access Protocol Version 1.0, IVOA Recommendation 27 March 2010
Epanechnikov, V. A. 1969, Theory of Probability & Its Applications, 14, 153
ESA 1997, The HIPPARCOS and TYCHO catalogues. Astrometric and photometric star catalogues derived from the ESA HIPPARCOS Space Astrometry Mission, ESA SP, 1200
Evans, D., Riello, M., De Angeli, F., et al. 2016, A&A, this volume
Eyer, L., Mowlavi, N., Evans, D. W., et al. 2016, A&A, this volume
Fabricius, C., Bastian, U., Portell, J., et al. 2016, A&A, this volume
Gould, A. 2004, ArXiv Astrophysics e-prints [arXiv:astro-ph/0403506]
Henden, A., & Munari, U. 2014, Contributions of the Astronomical Observatory Skalnate Pleso, 43, 518
Høg, E., Fabricius, C., Makarov, V. V., et al. 2000, A&A, 355, L27
Gaia Collaboration, Clementini, G., Eyer, E., et al. 2016a, A&A, this volume
Gaia Collaboration, Prusti, T., de Bruijne, J. H. J., et al. 2016b, A&A, this volume
Gaia Collaboration, van Leeuwen, F., Bastian, U., et al. 2016c, A&A, this volume
Jordi, C., Gebran, M., Carrasco, J. M., et al. 2010, A&A, 523, A48
Lindegren, L., Lammers, U., Bastian, U., Hernández, J., & Klioner, S. 2016, A&A, this volume
Lindegren, L., Lammers, U., Hobbs, D., et al. 2012, A&A, 538, A78
Mädler, T., Jofré, P., Gilmore, G., et al. 2016, A&A, in press DOI 10.1051/0004-6361/201629091
Marrese, P., & et al. 2016, A&A, this volume
Mason, B. D., Wycoff, G. L., Hartkopf, W. I., Douglass, G. G., & Worley, C. E. 2001, AJ, 122, 3466
Melis, C., Reid, M. J., Mioduszewski, A. J., Stauffer, J. R., & Bower, G. C. 2014, Science, 345, 1029
Michalik, D., & Lindegren, L. 2016, A&A, 586, A26
Michalik, D., Lindegren, L., & Hobbs, D. 2015, A&A, 574, A115
Mignard, F., Klioner, S., Lindegren, L., et al. 2016, A&A, this volume
Osuna, P., Ortiz, I., Lusted, J., et al. 2008, IVOA Astronomical Data Query Language Version 2.00, IVOA Recommendation 30 October 2008
Perryman, M. A. C., de Boer, K. S., Gilmore, G., et al. 2001, A&A, 369, 339
Recio-Blanco, A., de Laverny, P., Allende Prieto, C., et al. 2016, A&A, 585, A93
Riello, M., De Angeli, F., Evans, D. W., et al. 2016, A&A, this volume
Salgado, J., Berné, O., Adams, J. D., et al. 2016, A&A, this volume
Skrutskie, M. F., Cutri, R. M., Stiening, R., et al. 2006, AJ, 131, 1163
Smart, R. L., & Nicastro, L. 2014, A&A, 570, 8
van Leeuwen, F. 1999, A&A, 341, L71
van Leeuwen, F. 2007, HIPPARCOS, the New Reduction of the Raw Data, Astrophys. Space Sci. Lib., 350 edn. (Springer)
van Leeuwen, F. 2009, A&A, 497, 209
van Leeuwen, F., Evans, D. W., De Angeli, F., et al. 2016, A&A, this volume
Wenger, M., Ochsenbein, F., Egret, D., et al. 2000, A&AS, 143, 9
Whitmore, B. C., Allam, S. S., Budavári, T., et al. 2016, AJ, 151, 134
York, D. G., Adelman, J., Anderson, Jr., J. E., et al. 2000, AJ, 120, 1579

[1] Leiden Observatory, Leiden University, Niels Bohrweg 2, 2333 CA Leiden, The Netherlands
[2] INAF−Osservatorio astronomico di Padova, Vicolo Osservatorio 5, 35122 Padova, Italy
[3] Scientific Support Office, Directorate of Science, European Space Research and Technology Centre (ESA/ESTEC), Keplerlaan 1, 2201AZ Noordwijk, The Netherlands
[4] Laboratoire Lagrange, Université Nice Sophia-Antipolis, Observatoire de la Côte d'Azur, CNRS, CS 34229, 06304 Nice Cedex, France
[5] INAF−Osservatorio Astrofisico di Torino, via Osservatorio 20, 10025 Pino Torinese (TO), Italy
[6] GEPI, Observatoire de Paris, PSL Research University, CNRS, Univ. Paris Diderot, Sorbonne Paris Cité, 5 Place Jules Janssen, 92190 Meudon, France
[7] Max Planck Institute for Astronomy, Königstuhl 17, 69117 Heidelberg, Germany
[8] Astronomisches Rechen-Institut, Zentrum für Astronomie der Universität Heidelberg, Mönchhofstr, 12−14, 69120 Heidelberg, Germany
[9] Institute of Astronomy, University of Cambridge, Madingley Road, Cambridge CB3 0HA, UK
[10] Department of Astronomy, University of Geneva, Chemin des Maillettes 51, 1290 Versoix, Switzerland
[11] Mission Operations Division, Operations Department, Directorate of Science, European Space Research and Technology Centre (ESA/ESTEC), Keplerlaan 1, 2201 AZ, Noordwijk, The Netherlands
[12] Institut de Ciències del Cosmos, Universitat de Barcelona (IEEC-UB), Martí Franquès 1, 08028 Barcelona, Spain
[13] Lohrmann Observatory, Technische Universität Dresden, Mommsenstraße 13, 01062 Dresden, Germany
[14] European Space Astronomy Centre (ESA/ESAC), Camino bajo del Castillo, s/n, Urbanizacion Villafranca del Castillo, Villanueva de la Cañada, 28692 Madrid, Spain
[15] Lund Observatory, Department of Astronomy and Theoretical Physics, Lund University, Box 43, 22100 Lund, Sweden
[16] CNES Centre Spatial de Toulouse, 18 avenue Edouard Belin, 31401 Toulouse Cedex 9, France
[17] Institut d'Astronomie et d'Astrophysique, Université Libre de Bruxelles CP 226, Boulevard du Triomphe, 1050 Brussels, Belgium
[18] F.R.S.-FNRS, Rue d'Egmont 5, 1000 Brussels, Belgium
[19] INAF−Osservatorio Astrofisico di Arcetri, Largo Enrico Fermi 5, 50125 Firenze, Italy
[20] Telespazio Vega UK Ltd for ESA/ESAC, Camino bajo del Castillo, s/n, Urbanizacion Villafranca del Castillo, Villanueva de la Cañada, 28692 Madrid, Spain
[21] Laboratoire d'astrophysique de Bordeaux, Université de Bordeaux, CNRS, B18N, allée Geoffroy Saint-Hilaire, 33615 Pessac, France
[22] Instituut voor Sterrenkunde, KU Leuven, Celestijnenlaan 200D, 3001 Leuven, Belgium
[23] Department of Astrophysics/IMAPP, Radboud University Nijmegen, PO Box 9010, 6500 GL Nijmegen, The Netherlands
[24] Mullard Space Science Laboratory, University College London, Holmbury St. Mary, Dorking, Surrey RH5 6NT, UK
[25] Niels Bohr Institute, University of Copenhagen, Juliane Maries Vej 30, 2100 Copenhagen Ø, Denmark
[26] Centre for Electronic Imaging, Department of Physical Sciences, The Open University, Walton Hall MK7 6AA Milton Keynes, UK
[27] ALTEC S.p.a, Corso Marche, 79, 10146 Torino, Italy
[28] INAF−Osservatorio Astronomico di Bologna, via Ranzani 1, 40127 Bologna, Italy
[29] Serco Gestión de Negocios for ESA/ESAC, Camino bajo del Castillo, s/n, Urbanizacion Villafranca del Castillo, Villanueva de la Cañada, 28692 Madrid, Spain
[30] Department of Astronomy, University of Geneva, Chemin d'Ecogia 16, 1290 Versoix, Switzerland
[31] STFC, Rutherford Appleton Laboratory, Harwell, Didcot, OX11 0QX, UK
[32] Gaia DPAC Project Office, ESAC, Camino bajo del Castillo, s/n, Urbanizacion Villafranca del Castillo, Villanueva de la Cañada, 28692 Madrid, Spain
[33] SYRTE, Observatoire de Paris, PSL Research University, CNRS, Sorbonne Universités, UPMC Univ. Paris 06, LNE, 61 avenue de l'Observatoire, 75014 Paris, France
[34] National Observatory of Athens, I. Metaxa and Vas. Pavlou, Palaia Penteli, 15236 Athens, Greece
[35] IMCCE, Observatoire de Paris, PSL Research University, CNRS, Sorbonne Universités, UPMC Univ. Paris 06, Univ. Lille, 77 av. Denfert-Rochereau, 75014 Paris, France
[36] Royal Observatory of Belgium, Ringlaan 3, 1180 Brussels, Belgium
[37] Institut d'Astrophysique Spatiale, Université Paris XI, UMR 8617, CNRS, Bâtiment 121, 91405, Orsay Cedex, France
[38] Institute for Astronomy, Royal Observatory, University of Edinburgh, Blackford Hill, Edinburgh EH9 3HJ, UK
[39] HE Space Operations BV for ESA/ESAC, Camino bajo del Castillo, s/n, Urbanizacion Villafranca del Castillo, Villanueva de la Cañada, 28692 Madrid, Spain
[40] Institut d'Astrophysique et de Géophysique, Université de Liège, 19c, Allée du 6 Août, 4000 Liège, Belgium
[41] Área de Lenguajes y Sistemas Informáticos, Universidad Pablo de Olavide, Ctra. de Utrera, km 1, 41013 Sevilla, Spain
[42] Observatoire Astronomique de Strasbourg, Université de Strasbourg, CNRS, UMR 7550, 11 rue de l'Université, 67000 Strasbourg, France
[43] Kavli Institute for Cosmology, University of Cambridge, Madingley Road, Cambride CB3 0HA, UK
[44] Aurora Technology for ESA/ESAC, Camino bajo del Castillo, s/n, Urbanizacion Villafranca del Castillo, Villanueva de la Cañada, 28692 Madrid, Spain
[45] Laboratoire Univers et Particules de Montpellier, Université Montpellier, Place Eugène Bataillon, CC72, 34095 Montpellier Cedex 05, France
[46] Department of Astrophysics, Astronomy and Mechanics, National and Kapodistrian University of Athens, Panepistimiopolis, Zografos, 15783 Athens, Greece
[47] Department of Physics and Astronomy, Division of Astronomy and Space Physics, Uppsala University, Box 516, 75120 Uppsala, Sweden
[48] Università di Catania, Dipartimento di Fisica e Astronomia, Sezione Astrofisica, via S. Sofia 78, 95123 Catania, Italy
[49] INAF−Osservatorio Astrofisico di Catania, via S. Sofia 78, 95123 Catania, Italy
[50] Universidade da Coruña, Facultade de Informática, Campus de Elviña S/N, 15071, A Coruña, Spain
[51] CENTRA, Universidade de Lisboa, FCUL, Campo Grande, Edif. C8, 1749-016 Lisboa, Portugal
[52] University of Helsinki, Department of Physics, PO Box 64, 00014 University of Helsinki, Finland
[53] Finnish Geospatial Research Institute FGI, Geodeetinrinne 2, 02430 Masala, Finland
[54] Isdefe for ESA/ESAC, Camino bajo del Castillo, s/n, Urbanizacion Villafranca del Castillo, Villanueva de la Cañada, 28692 Madrid, Spain
[55] ASI Science Data Center, via del Politecnico SNC, 00133 Roma, Italy
[56] Institut UTINAM UMR6213, CNRS, OSU THETA Franche-Comté Bourgogne, Université Bourgogne Franche-Comté, 25000 Besançon, France
[57] Dpto. de Inteligencia Artificial, UNED, c/ Juan del Rosal 16, 28040 Madrid, Spain
[58] Elecnor Deimos Space for ESA/ESAC, Camino bajo del Castillo, s/n, Urbanizacion Villafranca del Castillo, Villanueva de la Cañada, 28692 Madrid, Spain
[59] Thales Services for CNES Centre Spatial de Toulouse, 18 avenue Edouard Belin, 31401 Toulouse Cedex 9, France
[60] EURIX S.r.l., via Carcano 26, 10153 Torino, Italy

[61] University of Vienna, Department of Astrophysics, Türkenschanzstraße 17, A1180 Vienna, Austria
[62] Department of Physics and Astronomy, The Johns Hopkins University, 3400 N Charles St, Baltimore, MD 21218, USA
[63] ON/MCTI-BR, Rua Gal. José Cristino 77, Rio de Janeiro, CEP 20921-400 RJ, Brazil
[64] OV/UFRJ-BR, Ladeira Pedro Antônio 43, Rio de Janeiro, CEP 20080-090 RJ, Brazil
[65] Faculdade Ciencias, Universidade do Porto, Departamento Matematica Aplicada, Rua do Campo Alegre, 687 4169-007 Porto, Portugal
[66] Instituto de Astrofísica e Ciências do Espa co, Universidade de Lisboa Faculdade de Ciências, Campo Grande, PT1749-016 Lisboa, Portugal
[67] Departamento de Astrofísica, Centro de Astrobiología (CSIC-INTA), ESA-ESAC. Camino Bajo del Castillo s/n. 28692 Villanueva de la Cañada, Madrid, Spain
[68] Department of Physics and Astronomy, University of Leicester, University Road, Leicester LE1 7RH, UK
[69] University of Oviedo, Campus Universitario, 33203 Gijón, Spain
[70] University of Cádiz, Avd. De la universidad, Jerez de la Frontera, 11002 Cádiz, Spain
[71] Kapteyn Astronomical Institute, University of Groningen, Landleven 12, 9747 AD Groningen, The Netherlands
[72] Consorci de Serveis Universitaris de Catalunya, C/ Gran Capità, 2−4 3rd floor, 08034 Barcelona, Spain
[73] University of Turin, Department of Computer Sciences, Corso Svizzera 185, 10149 Torino, Italy
[74] INAF−Osservatorio Astronomico di Roma, via di Frascati 33, 00078 Monte Porzio Catone (Roma), Italy
[75] CRAAG−Centre de Recherche en Astronomie, Astrophysique et Géophysique, Route de l'Observatoire Bp 63 Bouzareah 16340 Algiers, Algeria
[76] Universiteit Antwerpen, Onderzoeksgroep Toegepaste Wiskunde, Middelheimlaan 1, 2020 Antwerpen, Belgium
[77] Department of Physics and Astronomy, University of Padova, via Marzolo 8, 35131 Padova, Italy
[78] INAF−Osservatorio Astronomico di Teramo, via Mentore Maggini, 64100 Teramo, Italy
[79] INAF−Osservatorio Astronomico di Capodimonte, via Moiariello 16, 80131, Napoli, Italy
[80] Instituto de Astronomia, Geofìsica e Ciências Atmosféricas, Universidade de São Paulo, Rua do Matão, 1226 Cidade Universitaria, 05508-900 São Paulo, SP, Brazil
[81] Department of Geosciences, Tel Aviv University, 6997801 Tel Aviv, Israel
[82] Astronomical Institute Anton Pannekoek, University of Amsterdam, PO Box 94249, 1090 GE, Amsterdam, The Netherlands
[83] Leibniz Institute for Astrophysics Potsdam (AIP), An der Sternwarte 16, 14482 Potsdam, Germany
[84] ATOS for CNES Centre Spatial de Toulouse, 18 avenue Edouard Belin, 31401 Toulouse Cedex 9, France
[85] School of Physics and Astronomy, Tel Aviv University, 6997801 Tel Aviv, Israel
[86] UNINOVA – CTS, Campus FCT-UNL, Monte da Caparica, 2829-516 Caparica, Portugal
[87] Laboratoire Géoazur, Université Nice Sophia-Antipolis, UMR 7329, CNRS, Observatoire de la Côte d'Azur, 250 rue A. Einstein, 06560 Valbonne, France
[88] RHEA for ESA/ESAC, Camino bajo del Castillo, s/n, Urbanizacion Villafranca del Castillo, Villanueva de la Cañada, 28692 Madrid, Spain
[89] Astronomical Institute, Academy of Sciences of the Czech Republic, Fričova 298, 25165 Ondřejov, Czech Republic
[90] Barcelona Supercomputing Center – Centro Nacional de Supercomputación, c/ Jordi Girona 29, Ed. Nexus II, 08034 Barcelona, Spain
[91] Department of Mechanical Engineering, University of La Rioja, c/ San José de Calasanz, 31, 26004 Logroño, La Rioja, Spain
[92] ETSE Telecomunicación, Universidade de Vigo, Campus Lagoas-Marcosende, 36310 Vigo, Galicia, Spain
[93] SRON, Netherlands Institute for Space Research, Sorbonnelaan 2, 3584CA, Utrecht, The Netherlands
[94] Faculty of Mathematics and Physics, University of Ljubljana, Jadranska ulica 19, 1000 Ljubljana, Slovenia
[95] Physics Department, University of Antwerp, Groenenborgerlaan 171, 2020 Antwerp, Belgium
[96] Harvard-Smithsonian Center for Astrophysics, 60 Garden Street, Cambridge MA 02138, USA
[97] Institut de Physique de Rennes, Université de Rennes 1, 35042 Rennes, France
[98] Shanghai Astronomical Observatory, Chinese Academy of Sciences, 80 Nandan Rd, 200030 Shanghai, PR China
[99] CSC Danmark A/S, Retortvej 8, 2500 Valby, Denmark
[100] Las Cumbres Observatory Global Telescope Network, Inc., 6740 Cortona Drive, Suite 102, Goleta, CA 93117, USA
[101] Astrophysics Research Institute, Liverpool John Moores University, L3 5RF, UK
[102] Konkoly Observatory, Research Centre for Astronomy and Earth Sciences, Hungarian Academy of Sciences, Konkoly Thege Miklós út 15−17, 1121 Budapest, Hungary
[103] Baja Observatory of University of Szeged, Szegedi út III/70, 6500 Baja, Hungary
[104] Laboratoire AIM, IRFU/Service d'Astrophysique – CEA/DSM – CNRS – Université Paris Diderot, Bât 709, CEA-Saclay, 91191 Gif-sur-Yvette Cedex, France
[105] INAF−Osservatorio Astronomico di Trieste, via G.B. Tiepolo 11, 34143 Trieste, Italy
[106] Laboratoire de l'Accélérateur Linéaire, Université Paris-Sud, CNRS/IN2P3, Université Paris-Saclay, 91898 Orsay Cedex, France
[107] École polytechnique fédérale de Lausanne, SB MATHAA STAP, MA B1 473 (Bâtiment MA), Station 8, 1015 Lausanne, Switzerland
[108] INAF/IASF-Bologna, via P. Gobetti 101, 40129 Bologna, Italy
[109] Technical University of Madrid, José Gutiérrez Abascal 2, 28006 Madrid, Spain
[110] EQUERT International for CNES Centre Spatial de Toulouse, 18 avenue Edouard Belin, 31401 Toulouse Cedex 9, France
[111] AKKA for CNES Centre Spatial de Toulouse, 18 avenue Edouard Belin, 31401 Toulouse Cedex 9, France
[112] Villanova University, Dept. of Astrophysics and Planetary Science, 800 E Lancaster Ave, Villanova PA 19085, USA
[113] Vitrociset Belgium for ESA/ESAC, Camino bajo del Castillo, s/n, Urbanizacion Villafranca del Castillo, Villanueva de la Cañada, 28692 Madrid, Spain
[114] Fork Research, Rua do Cruzado Osberno, Lt. 1, 9 esq., Lisboa, Portugal
[115] APAVE SUDEUROPE SAS for CNES Centre Spatial de Toulouse, 18 avenue Edouard Belin, 31401 Toulouse Cedex 9, France
[116] Spanish Virtual Observatory
[117] Fundación Galileo Galilei – INAF, Rambla José Ana Fernández Pérez 7, 38712 Breña Baja, Santa Cruz de Tenerife, Spain
[118] INSA for ESA/ESAC, Camino bajo del Castillo, s/n, Urbanizacion Villafranca del Castillo, Villanueva de la Cañada, 28692 Madrid, Spain
[119] Dpto. Arquitectura de Computadores y Automática, Facultad de Informática, Universidad Complutense de Madrid, C/ Prof. José García Santesmases s/n, 28040 Madrid, Spain
[120] H H Wills Physics Laboratory, University of Bristol, Tyndall Avenue, Bristol BS8 1TL, UK
[121] Stellar Astrophysics Centre, Aarhus University, Department of Physics and Astronomy, 120 Ny Munkegade, Building 1520, 8000 Aarhus C, Denmark
[122] Applied Physics Department, University of Vigo, 36310 Vigo, Spain
[123] HE Space Operations BV for ESA/ESTEC, Keplerlaan 1, 2201AZ, Noordwijk, The Netherlands
[124] Warsaw University Observatory, Al. Ujazdowskie 4, 00-478 Warszawa, Poland

[125] Instituto de Astrofísica de Canarias, 38205 La Laguna, Tenerife, Spain
[126] Universidad de La Laguna, Departamento de Astrofísica, 38206 La Laguna, Tenerife, Spain
[127] RHEA for ESA/ESTEC, Keplerlaan 1, 2201AZ Noordwijk, The Netherlands
[128] Max Planck Institute for Solar System Research, Justus-von-Liebig-Weg 3, 37077 Göttingen, Germany
[129] SISSA (Scuola Internazionale Superiore di Studi Avanzati), via Bonomea 265, 34136 Trieste, Italy
[130] Instituto Nacional de Pesquisas Espaciais/Ministério da Ciencia Tecnologia, Avenida dos Astronautas 1758, SP 12227-010, São José Dos Campos, Brazil
[131] Argelander Institut für Astronomie der Universität Bonn, Auf dem Hügel 71, 53121 Bonn, Germany
[132] European Southern Observatory (ESO), Karl-Schwarzschild-Straße 2, 85748 Garching bei München, Germany
[133] Laboratory of Optics, Lasers and Systems, Faculty of Sciences, University of Lisbon, Campus do Lumiar, Estrada do Paço do Lumiar, 22, 1649-038 Lisboa, Portugal
[134] Department of Physics and Astronomy, Notre Dame University, Louaize, PO Box 72, Zouk Mikaël, Lebanon
[135] University of Nova Gorica, Vipavska 13, 5000 Nova Gorica, Slovenia
[136] Max Planck Institute for Extraterrestrial Physics, OPINAS, Gießenbachstraße, 85741 Garching, Germany
[137] NASA/IPAC Infrared Science Archive, California Institute of Technology, Mail Code 100-22, 770 South Wilson Avenue, Pasadena, CA, 91125, USA
[138] Center of Applied Space Technology and Microgravity (ZARM), c/o Universität Bremen, Am Fallturm 1, 28359 Bremen, Germany
[139] RHEA System for ESA/ESOC, Robert Bosch Straße 5, 64293 Darmstadt, Germany
[140] Tartu Observatory, 61602 Tõravere, Estonia
[141] Sydney Institute for Astronomy, School of Physics A28, The University of Sydney, NSW 2006, Australia
[142] Slovak Organisation for Space Activities, Zamocka 18, 85101 Bratislava, Slovak Republic
[143] National Astronomical Observatories, CAS, 100012 Beijing, PR China
[144] US Naval Observatory, Astrometry Department, 3450 Massachusetts Ave. NW, Washington DC 20392-5420 D.C., USA
[145] European Southern Observatory (ESO), Alonso de Córdova 3107, Vitacura, Casilla 19001, Santiago de Chile, Chile
[146] Airbus Defence and Space SAS, 31 Rue des Cosmonautes, 31402 Toulouse Cedex 4, France
[147] EJR-Quartz BV for ESA/ESTEC, Keplerlaan 1, 2201AZ, Noordwijk, The Netherlands
[148] The Server Labs for ESA/ESAC, Camino bajo del Castillo, s/n, Urbanizacion Villafranca del Castillo, Villanueva de la Cañada, 28692 Madrid, Spain
[149] Astronomical Observatory Institute, Faculty of Physics, A. Mickiewicz University, ul. Słoneczna 36, 60-286 Poznań, Poland
[150] CS Systèmes d'Information for CNES Centre Spatial de Toulouse, 18 avenue Edouard Belin, 31401 Toulouse Cedex 9, France
[151] Directorate of Science, European Space Research and Technology Centre (ESA/ESTEC), Keplerlaan 1, 2201AZ, Noordwijk, The Netherlands
[152] Praesepe BV for ESA/ESAC, Camino bajo del Castillo, s/n, Urbanizacion Villafranca del Castillo, Villanueva de la Cañada, 28692 Madrid, Spain
[153] Sorbonne Universités UPMC et CNRS, UMR7095, Institut d'Astrophysique de Paris, 75014 Paris, France
[154] GMV for ESA/ESAC, Camino bajo del Castillo, s/n, Urbanizacion Villafranca del Castillo, Villanueva de la Cañada, 28692 Madrid, Spain
[155] Institute of Theoretical Physics and Astronomy, Vilnius University, Sauletekio al. 3, Vilnius, LT-10222, Lithuania
[156] S[&]T Corporation, PO Box 608, 2600 AP, Delft, The Netherlands
[157] Department of Space Studies, Southwest Research Institute (SwRI), 1050 Walnut Street, Suite 300, Boulder, Colorado 80302, USA
[158] Deutsches Zentrum für Luft- und Raumfahrt, Institute of Space Systems, Am Fallturm 1, 28359 Bremen, Germany
[159] University of Applied Sciences Munich, Karlstr. 6, 80333 Munich, Germany
[160] Dipartimento di Fisica, Università di Roma Tor Vergata, via della Ricerca Scientifica 1, 00133 Rome, Italy
[161] Department of Physics and Astronomy, University of the Western Cape, Robert Sobukwe Road, 7535 Bellville, Cape Town, South Africa
[162] INAF−Istituto di Radioastronomia, via Gobetti 101, 40129 Bologna, Italy
[163] Department of Physics, Florida International University, 11200 SW 8th Street, Miami, FL 33199, USA
[164] Hamburger Sternwarte, Gojenbergsweg 112, 21029 Hamburg, Germany

Appendix A: List of acronyms

Table A.1. List of acronyms used in this paper.

Acronym	Description
2MASS	Two-Micron All Sky Survey
AAVSO	American Association of Variable Star Observers
APASS	AAVSO Photometric All-Sky Survey
BP	Blue Photometer
CCD	Charge-Coupled Device
CTI	Charge Transfer Inefficiency
DPAC	Data Processing and Analysis Consortium
ICRF	International Celestial Reference Frame
IGSL	Initial *Gaia* Source List
OBMT	On-Board Mission Timeline
PSF	Point Spread Function
RP	Red Photometer
RVS	Radial Velocity Spectrometer
TCB	Barycentric Coordinate Time
TDI	Time-Delayed Integration (CCD)
TGAS	*Tycho-Gaia* Astrometric Solution

Appendix B: Example *Gaia* archive queries

Tables B.1–B.3 list the queries in Astronomical Data Query Language form that can be submitted to the *Gaia* archive in order to retrieve the data necessary to reproduce Figs. 3, 4, 5, 9, and 6. The selection on the standard uncertainty in G ignores the contribution of the G-band magnitude zero point error. Including this small (∼0.003 mag) error term does not alter the query results, except for the selection for Fig. 5.

Table B.1. Minimal queries that can be submitted to the *Gaia* archive in the Astronomical Data Query Language to retrieve the data necessary to reproduce the HR diagrams and the magnitude distribution in Figs. 3 and 4.

Query to reproduce panels **a** and **b** of Fig. 3. This results in a table of 43 546 rows listing the *Gaia* source identifier, the HIPPARCOS number, the values of M_G based on the HIPPARCOS and *Gaia* DR1 parallaxes respectively, and the value of $(B-V)$ from the HIPPARCOS catalogue (van Leeuwen 2007).

```
select gaia.source_id, gaia.hip,
  gaia.phot_g_mean_mag+5*log10(gaia.parallax)-10 as g_mag_abs_gaia,
  gaia.phot_g_mean_mag+5*log10(hip.plx)-10 as g_mag_abs_hip,
  hip.b_v
from gaiadr1.tgas_source as gaia
inner join gaiadr1.hipparcos_newreduction as hip
  on gaia.hip = hip.hip
where gaia.parallax/gaia.parallax_error >= 5 and
  hip.plx/hip.e_plx >= 5 and
  hip.e_b_v > 0.0 and hip.e_b_v <= 0.05 and
  2.5/log(10)*gaia.phot_g_mean_flux_error/gaia.phot_g_mean_flux <= 0.05
```

Query to reproduce panel **c** of Fig. 3. This results in a table of 74 771 rows listing the *Gaia* source identifier, the values of M_G based on the *Gaia* DR1 parallax, and the value of $(B-V)$ from the HIPPARCOS catalogue (van Leeuwen 2007).

```
select gaia.source_id, gaia.hip,
  gaia.phot_g_mean_mag+5*log10(gaia.parallax)-10 as g_mag_abs,
  hip.b_v
from gaiadr1.tgas_source as gaia
inner join gaiadr1.hipparcos_newreduction as hip
  on gaia.hip = hip.hip
where gaia.parallax/gaia.parallax_error >= 5 and
  hip.e_b_v > 0.0 and hip.e_b_v <= 0.05 and
  2.5/log(10)*gaia.phot_g_mean_flux_error/gaia.phot_g_mean_flux <= 0.05
```

Query to reproduce Fig. 4. This results in a table of 3174 rows listing the *Gaia* source identifier, and the values of M_G based on the *Gaia* DR1 and HIPPARCOS (van Leeuwen 2007) parallaxes, respectively.

```
select gaia.source_id, gaia.hip,
  gaia.phot_g_mean_mag+5*log10(gaia.parallax)-10 as g_mag_abs_gaia,
  gaia.phot_g_mean_mag+5*log10(hip.plx)-10 as g_mag_abs_hip
from gaiadr1.tgas_source as gaia
inner join gaiadr1.hipparcos_newreduction as hip
  on gaia.hip = hip.hip
where gaia.parallax/gaia.parallax_error >= 5 and
  hip.plx/hip.e_plx >= 5 and
  hip.e_b_v > 0.0 and hip.e_b_v <= 0.05 and
  hip.b_v >= 1.0 and hip.b_v <= 1.1 and
  2.5/log(10)*gaia.phot_g_mean_flux_error/gaia.phot_g_mean_flux <= 0.05
```

Table B.2. Minimal queries that can be submitted to the *Gaia* archive in the Astronomical Data Query Language to retrieve the data necessary to reproduce the HR diagram in Fig. 5 as well as the Pleiades parallax histogram in Fig. 9.

Query to reproduce Fig. 5. This results in a table of 1 004 207 rows (1 004 204 when including the zero-point uncertainty on G in the selection criteria) listing the *Gaia* source identifier and the values of M_G and $(G - K_s)$.

```
select gaia.source_id,
  gaia.phot_g_mean_mag+5*log10(gaia.parallax)-10 as g_mag_abs,
  gaia.phot_g_mean_mag-tmass.ks_m as g_min_ks
from gaiadr1.tgas_source as gaia
inner join gaiadr1.tmass_best_neighbour as xmatch
  on gaia.source_id = xmatch.source_id
inner join gaiadr1.tmass_original_valid as tmass
  on tmass.tmass_oid = xmatch.tmass_oid
where gaia.parallax/gaia.parallax_error >= 5 and ph_qual = 'AAA' and
  sqrt(power(2.5/log(10)*gaia.phot_g_mean_flux_error/gaia.phot_g_mean_flux,2)) <= 0.05 and
  sqrt(power(2.5/log(10)*gaia.phot_g_mean_flux_error/gaia.phot_g_mean_flux,2)
       + power(tmass.ks_msigcom,2)) <= 0.05
```

Query to carry out a simplistic selection of Pleiades cluster members and reproduce Fig. 9. This results in a table of 164 rows listing the *Gaia* source identifier and the *Gaia* parallax.

```
select gaia.source_id,
  gaia.parallax
from gaiadr1.tgas_source as gaia
where contains(point('ICRS',gaia.ra,gaia.dec),circle('ICRS',56.75,24.12,5)) = 1
  and sqrt(power(gaia.pmra-20.5,2)+power(gaia.pmdec+45.5,2)) < 6.0
```

Table B.3. Minimal queries that can be submitted to the *Gaia* archive in the Astronomical Data Query Language to retrieve the data necessary to reproduce the HR diagram in Fig. 6. In this case the query is split into three parts.

Query to retrieve stars with HIPPARCOS colour indices. This results in a table of 30 009 rows listing the *Gaia* source identifier, the value of M_G based on the *Gaia* DR1 parallax, the HIPPARCOS (van Leeuwen 2007) value of $(B-V)$, and the value of $v_\perp$.

```
select gaia.source_id,
  gaia.phot_g_mean_mag+5*log10(gaia.parallax)-10 as g_mag_abs,
  hip.b_v as b_min_v,
  sqrt(power(gaia.pmra,2)+power(gaia.pmdec,2))/gaia.parallax*4.74047 as vperp
from gaiadr1.tgas_source as gaia
inner join gaiadr1.hipparcos_newreduction as hip
  on gaia.hip = hip.hip
where gaia.parallax/gaia.parallax_error >= 5 and
  hip.e_b_v > 0.0 and hip.e_b_v <= 0.05 and
  2.5/log(10)*gaia.phot_g_mean_flux_error/gaia.phot_g_mean_flux <= 0.05 and
  (gaia.parallax >= 10.0 or
  sqrt(power(gaia.pmra,2)+power(gaia.pmdec,2)) >= 200 or
  gaia.phot_g_mean_mag <= 7.5)
```

Query to retrieve stars with *Tycho*-2 colour indices. This results in a table of 8983 rows listing the *Gaia* source identifier, the value of M_G based on the *Gaia* DR1 parallax, the *Tycho*-2 value of $(B-V)$ calculated as $0.85(B-V)_\mathrm{T}$, and the value of $v_\perp$.

```
select gaia.source_id,
  gaia.phot_g_mean_mag+5*log10(gaia.parallax)-10 as g_mag_abs,
  0.85*(tycho2.bt_mag-tycho2.vt_mag) as b_min_v,
  sqrt(power(gaia.pmra,2)+power(gaia.pmdec,2))/gaia.parallax*4.74047 as vperp
from gaiadr1.tgas_source as gaia
inner join gaiadr1.tycho2 as tycho2
  on gaia.tycho2_id = tycho2.id
where gaia.parallax/gaia.parallax_error >= 5 and
  sqrt(power(tycho2.e_bt_mag,2) + power(tycho2.e_vt_mag,2)) <= 0.05 and
  2.5/log(10)*gaia.phot_g_mean_flux_error/gaia.phot_g_mean_flux <= 0.05 and
  (gaia.parallax >= 10.0 or
  sqrt(power(gaia.pmra,2)+power(gaia.pmdec,2)) >= 200 or
  gaia.phot_g_mean_mag <= 7.5)
```

Query to retrieve stars with APASS colour indices. This results in a table of 2144 rows listing the *Gaia* source identifier, the value of M_G based on the *Gaia* DR1 parallax, the APASS value of $(B-V)$, and the value of $v_\perp$.

```
select gaia.source_id,
  gaia.phot_g_mean_mag+5*log10(gaia.parallax)-10 as g_mag_abs,
  (urat.b_mag-urat.v_mag) as b_min_v,
  sqrt(power(gaia.pmra,2)+power(gaia.pmdec,2))/gaia.parallax*4.74047 as vperp
from gaiadr1.tgas_source as gaia
inner join gaiadr1.tycho2 as tycho2
  on gaia.tycho2_id = tycho2.id
inner join gaiadr1.urat1_best_neighbour as uratxmatch
  on gaia.source_id = uratxmatch.source_id
inner join gaiadr1.urat1_original_valid as urat
  on uratxmatch.urat1_oid = urat.urat1_oid
where gaia.parallax/gaia.parallax_error >= 5 and
  sqrt(power(tycho2.e_bt_mag,2) + power(tycho2.e_vt_mag,2)) > 0.05 and
  sqrt(power(urat.b_mag_error,2) + power(urat.v_mag_error,2)) <= 0.05 and
  2.5/log(10)*gaia.phot_g_mean_flux_error/gaia.phot_g_mean_flux <= 0.05 and
  (gaia.parallax >= 10.0 or
  sqrt(power(gaia.pmra,2)+power(gaia.pmdec,2)) >= 200 or
  gaia.phot_g_mean_mag <= 7.5)
```